NTT Technical Review

2
2012

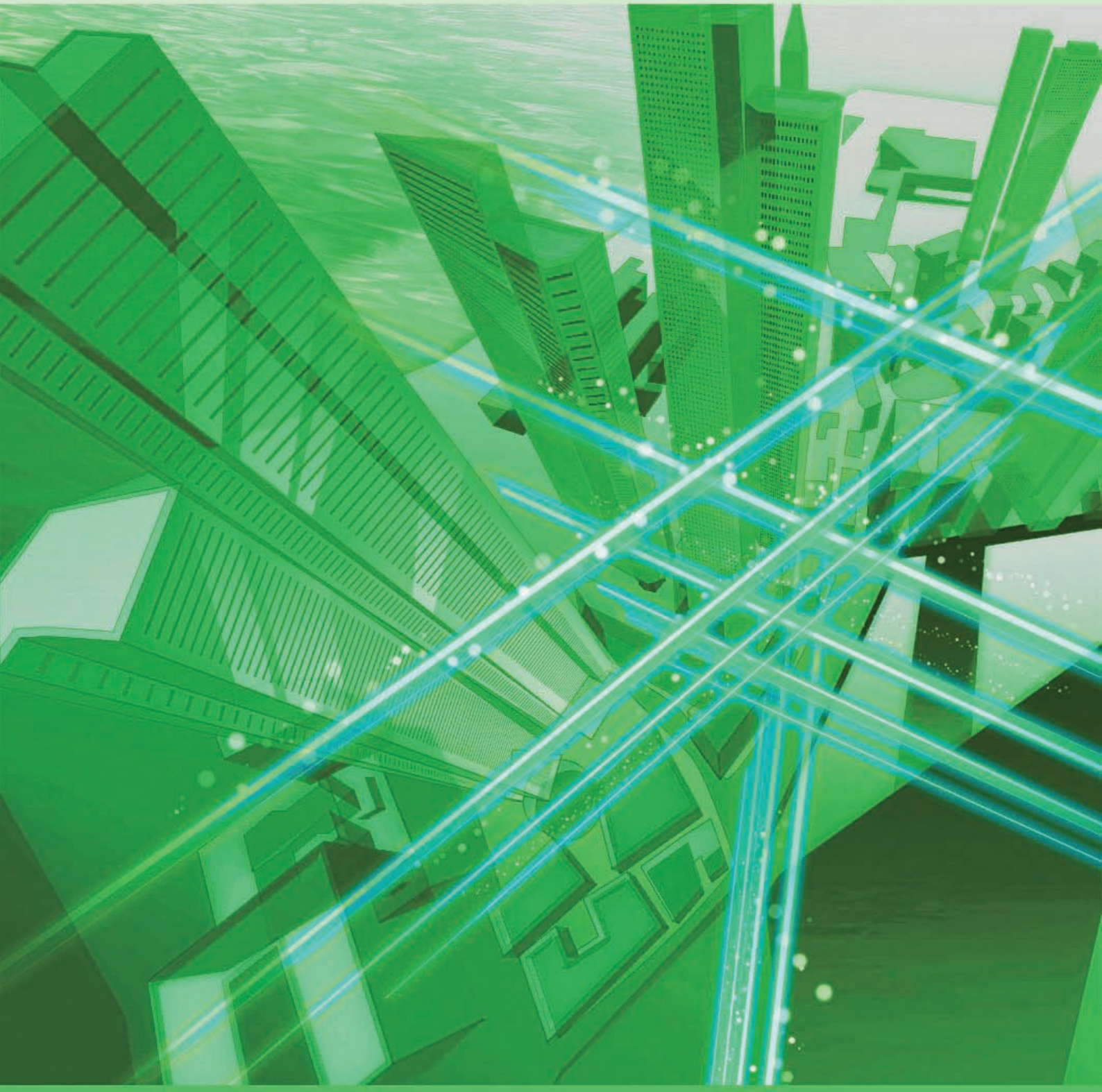

February 2012 Vol. 10 No. 2

NTT Technical Review

February 2012 Vol. 10 No. 2

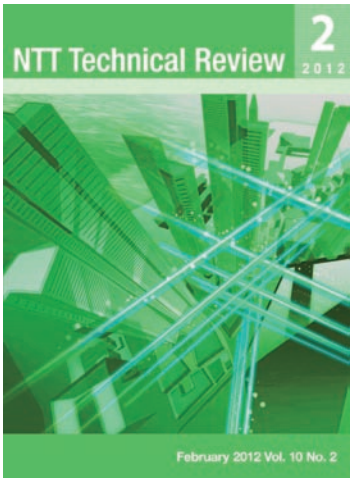

NTT R&D of Systems and Devices for Safety

Kimihisa Aihara† *and Naoya Kukutsu*

Abstract

In this article, we introduce NTT's research and development (R&D) of imaging and sensing technology for *making the hidden visible* in order to make our lives safe.

1. Introduction

Since the major earthquake that occurred in eastern Japan last year (on March 11, 2011), expectations for technology that supports safety in our lives have increased. NTT has long been engaged in four broad fields of research and development (R&D) related to imaging and sensing technology to support safety from the viewpoints of meeting current needs and sowing seeds for the future (**Fig. 1**).

Representative of the former viewpoint is R&D of facility management for the maintenance and management of basic communication facilities, particularly aiming for greater accuracy and efficiency in the inspection and diagnosis of concrete structures such as concrete poles, cable tunnels, and office buildings.

For the latter, there is R&D of new imaging and sensing technology that uses terahertz waves, which occupy a frequency band that is currently undeveloped for basic communication technology. Lying between radio waves and visible light in the electromagnetic spectrum, terahertz waves hold promise for contributing to a safer and more secure society through skillful use of the features of both radio and light. They allow the implementation of new application fields that have previously been impossible, such as remote gas sensing and spectroscopic analysis [1], [2]. Another example is technology for detecting harmful substances based on NTT's own μTAS (micro-total analysis system), which uses ultraviolet region spectroscopic analysis technology [3]. In those R&D activities, repeated simulations based on theory and measurements are used to understand electromagnetic wave propagation or gas flow path behavior for application in device design and manufacture. Furthermore, the sensitivity of sensing and analysis is improved by the addition of signal processing, with the result that these various systems are almost ready for use.

In this article, we describe our efforts in the above-mentioned areas.

2. Concrete structure crack detection technology

NTT maintains a nationwide network of concrete poles, cable tunnels, office buildings, and other concrete structures that support communication services. Those facilities were mainly constructed during the period of rapid growth, so many of them are over 40 years old and are beginning to deteriorate. This situation has made facility management an important issue.

The position of current concrete pole inspection methods and current R&D of new inspection methods is illustrated in **Fig. 2**. Here, we introduce image analysis and millimeter-wave imaging techniques for crack detection.

Surface cracking in concrete structures allows moisture to enter and corrode the iron reinforcement bars inside, reducing the strength of the structure. For that reason, information about the presence of surface cracks and their number, widths, and lengths is important for structural integrity evaluation.

† NTT Microsystem Integration Laboratories
Atsugi-shi, 243-0198 Japan

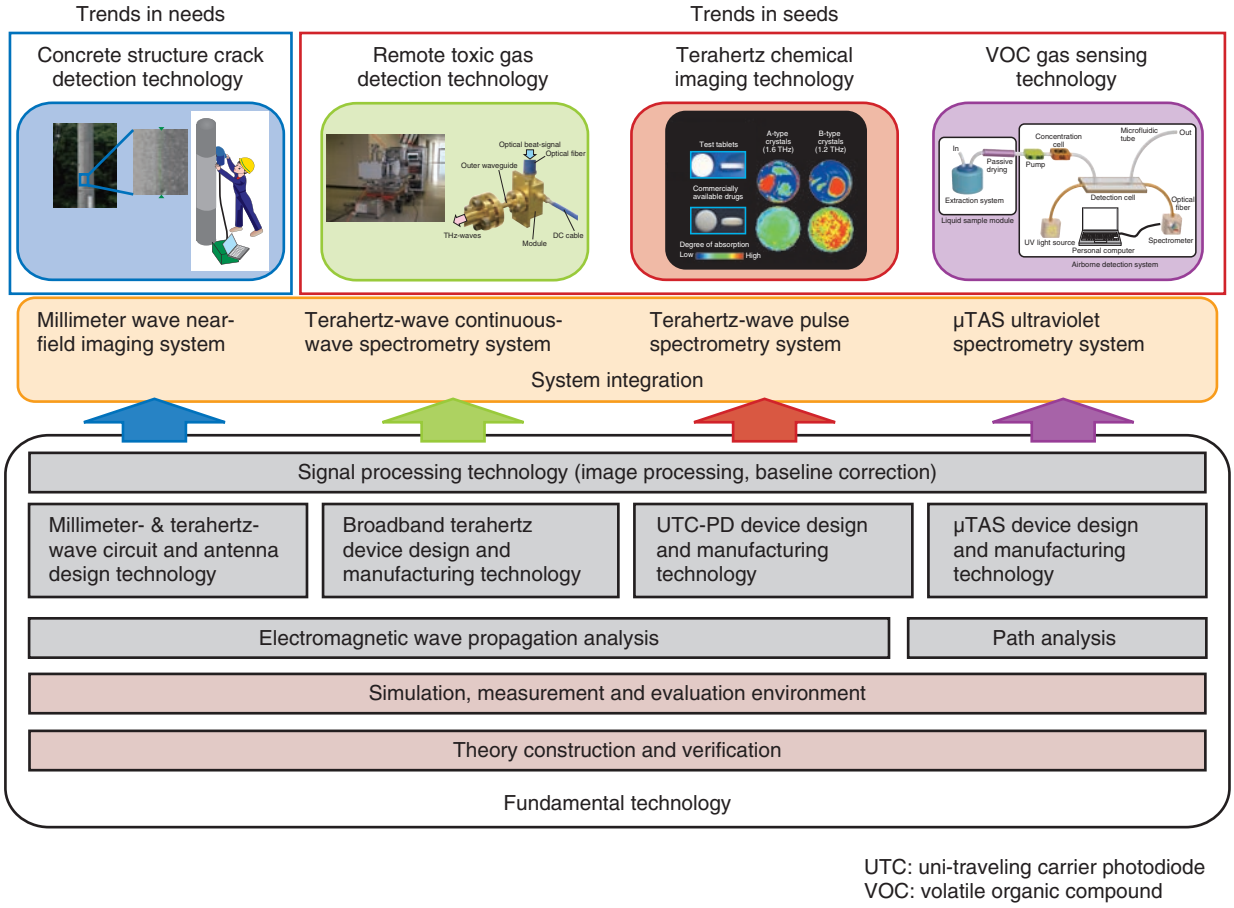

UTC: uni-traveling carrier photodiode
VOC: volatile organic compound

Fig. 1. Imaging and sensing technology supporting safety and security.

NTT EAST and NTT WEST together manage about 11.85 million concrete poles. Because pole inspections to detect cracking are currently done visually by workers, there is a need to develop a more efficient inspection method. Automatic crack detection by image analysis is a technique that could meet this need. However, concrete poles have foot pegs, belts, plates, and other items attached to them that hinder image analysis, so commercial software has a high rate of error in crack detection.

To solve that problem, NTT is developing automatic crack detection software that can reduce the detection errors caused by such obstacles by applying an obstacle removal algorithm and a neural network for crack shape recognition. That R&D is described in detail in the Feature Article "Detection of Cracks in Concrete Structures from Digital Camera Images" in this issue [4].

Some concrete poles have plastic sheeting attached to them to prevent unwanted posters being pasted there (bill-posting prevention sheets). Since the sheeting blocks the concrete surface from view, ultrasonic inspection equipment (pole tester) is used. However, ultrasonic inspection has difficulty detecting fine cracks. Moreover, the surfaces of many concrete structures other than poles are often painted, wallpapered, tiled, or covered with reinforcing material that makes visual inspection difficult. Techniques for detecting cracks below such coverings include the use of ultrasonic waves and x-rays, which can pass through the coverings. Ultrasonic waves are used to measure cracks that are more than one millimeter wide, but that resolution is insufficient for early detection of cracking in concrete poles, which requires the detection of submillimeter cracks. X-rays have an extremely short wavelength that allows high resolution, but x-ray inspection requires the object to be inspected to be located between a transmitter and a receiver. Moreover, x rays are harmful to humans, so x-ray equipment is difficult to use for

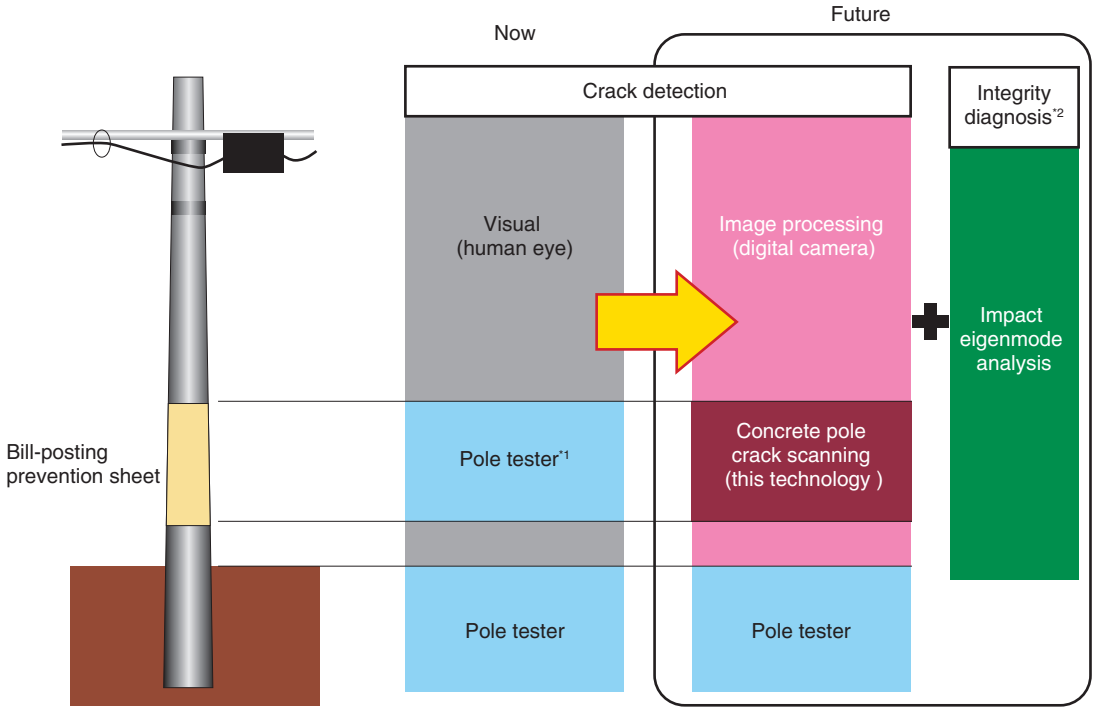

*1 Probes are positioned above and below the bill-posting prevention sheet, but this results in a long ultrasonic wave propagation path (about 2 m), so the accuracy is low and it is difficult to detect fine cracks.
*2 Broken rebar diagnosis equipment that uses impact eigenmode analysis is currently being developed by NTT Access Network Service Systems Laboratories.

Fig. 2. NTT concrete pole inspection technology.

inspections conducted in the field.

To solve that problem, NTT has investigated imaging techniques that use millimeter waves (77-GHz-band electromagnetic waves) to *see* what is hidden from the unaided eye. That work has resulted in the development of a portable scanner that can observe the condition of the pole surface lying beneath a bill-posting prevention sheet or other such covering. This R&D is explained in detail in the Feature Article "Millimeter-wave Imaging for Detecting Surface Cracks on Concrete Pole Covered with Bill-posting Prevention Sheet" [5]. It introduces technology for detecting surface cracks in concrete structures caused by broken rebar, but NTT Access Network Service Systems Laboratories has also been developing techniques that use impact mode analysis for diagnosing rebar deterioration.

3. Basic technology for terahertz wave signals

Terahertz waves are electromagnetic waves in the frequency range from 300 GHz to 3 THz (wavelength: from 100 μm to 1 mm). They have the ability to pass through some materials and exhibit absorption lines that are specific to the material. These characteristics can be used to identify materials. Another feature is that this radiation is not as harmful to the human body as x-rays are. If these features can be applied to imaging and sensing, they will make it possible to obtain new data that cannot be gathered by conventional techniques that use x-rays, infrared radiation, or microwaves, and we can expect many applications. What has prevented industrial applications so far is that it is very difficult to generate sufficiently strong terahertz waves over a wide frequency range by using electrical technology. The reason is that no efficient means of generating terahertz-band electromagnetic waves has been established because these waves exceed the operating frequencies of transistors and other active devices [6].

NTT has applied many years of optical communication R&D to develop new technology that uses a uni-traveling carrier photodiode (UTC-PD). The UTC-PD, which features an extremely fast response,

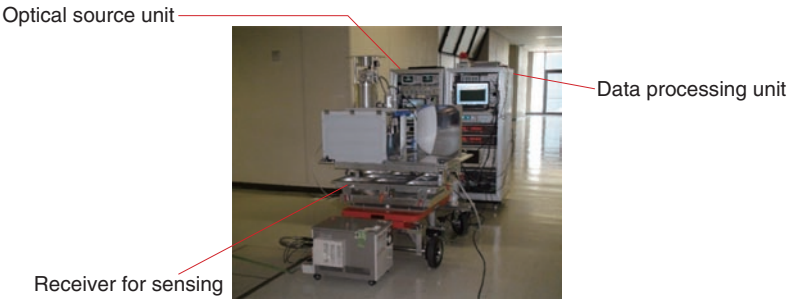

Fig. 3. Remote gas detection equipment.

was originally developed for use in communications to convert an optical signal into an electrical signal. The new UTC-PD-based terahertz-wave generator uses a UTC-PD to convert an optical signal into an electrical one, which is then converted to produce terahertz waves [7]. This technique uses the stable, broadband, ultrahigh-frequency characteristics of photonics to generate terahertz-band electromagnetic waves for various applications. In this way, imaging and sensing with this frequency band is made feasible. This R&D is explained in detail in the Feature Article "Development of Terahertz-wave Photomixer Module Using a Uni-travelling-carrier Photodiode" [8].

4. Remote detection of dangerous gases with terahertz waves

At the site of fires or other disasters, a rapid response is needed to prevent secondary damage. There is thus a pressing demand for the development of systems that can detect carbon monoxide, hydrogen cyanide, and other dangerous gases from a remote location.

NTT is engaged in R&D for applying its terahertz-wave generation technology to the remote detection of dangerous gases (**Fig. 3**). Terahertz waves differ from light in that they are not scattered by dust or smoke and they can propagate through a fire without any significant attenuation. Moreover, because terahertz waves resonate at a frequency of rotation and vibration of gas molecules, dangerous gases have specific absorption spectra for this frequency band, and the absorption line patterns can be used to identify the types of gases present. These properties can be used to detect toxic gases from a safe distance, even under conditions of extremely low visibility due to smoke etc.

NTT has developed a prototype system for remotely detecting dangerous gases under a commission from the National Institute of Information and Communications Technology and in cooperation with the University of Tokyo, the National Institute of Advanced Industrial Science and Technology, the Spectra Design Company, and others. This system was tested and evaluated in a full-scale simulated fire environment at the Fire Research and Test Laboratory of Tokyo University of Science. The tests verified the system's effectiveness for remotely detecting hydrogen cyanide gas as an example of a dangerous gas. This R&D is described in detail in the Feature Article "Remote Detection of Hazardous Gases in Full-scale Simulated Fire by Using Terahertz Electromagnetic Waves" [9].

5. Terahertz spectroscopy

Terahertz spectroscopy is an analytical chemistry technique that identifies substances by detecting hydrogen bonds and hydrate bonds and their interactions with other molecules [2] (**Fig. 4**).

By improving the latest terahertz-frequency components such as ultrashort-pulse lasers and photoconductive antennas, we are approaching realistic terahertz chemical imaging (TCI) and analysis technology. Because TCI can clarify the distribution of hydrogen bonds and molecular networks, it is expected to be a powerful tool for biology, pharmacology, and the life sciences. TCI technology can determine the two-dimensional distribution of molecules on the basis of molecular networks revealed by terahertz-wave absorption spectra. As an application to actual pharmaceutical molecules, two polymorphs of famotidine, a component of histamine receptor antagonist (H2 blocker) antacids, have been distinguished in pills. Polymorphs are composed of the same

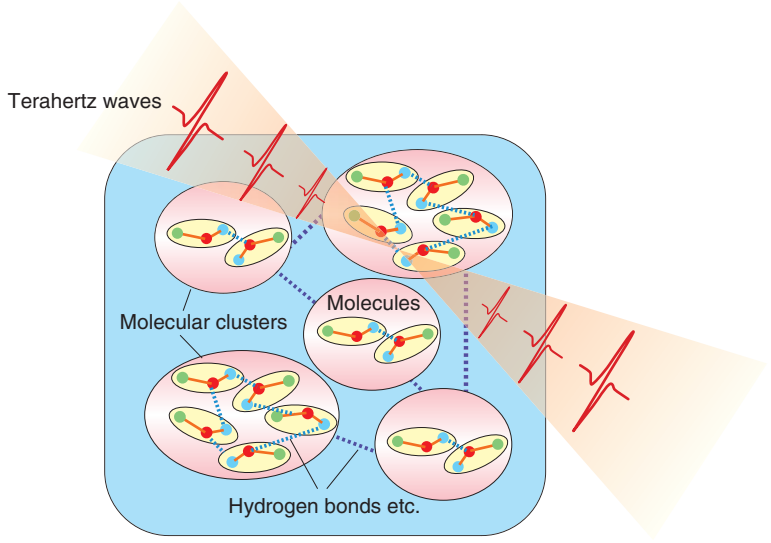

Fig. 4. Concept of terahertz spectroscopy.

molecules, but differ in how these molecules are linked. Large differences in the effectiveness of polymorphic drugs due to differences in chemical properties have been reported. New detection methods thus have major significance for the development of even safer pharmaceuticals.

This R&D is described in more detail in the Feature Article "Visualization of Pharmaceutical Drug Molecules by Terahertz Chemical Imaging" [10].

6. VOC gas sensing by ultraviolet absorption spectrometry

The Ministry of the Environment has established standards for benzene, toluene, xylene, and other highly toxic, aromatic, volatile organic compounds (VOCs) as dangerous gases in our environment besides combustion gases such as carbon monoxide and hydrogen cyanide to which terahertz waves have been applied for remote detection. The sources of those toxic gases include gasoline stations, printing shops, paint shops, and other small-scale facilities as well as large-scale facilities such as chemical plants, steelmaking plants, oil refineries, and power plants. Such facilities may release even larger amounts of dangerous materials into the atmosphere during an earthquake or fire. Those pollutants, together with radioactive pollution, are becoming a cause of serious environmental pollution. Besides earthquakes and other disasters, the deterioration of gasoline station facilities with age and other such situations present the danger of toxins leaking onto the ground surface or into groundwater. The methods of detecting such dangerous substances have generally been analytical ones that combine gas chromatography and mass spectroscopy. Such methods are performed in laboratories and require a large amount of equipment. They also rely on manual collection of gas samples. All of these factors hinder immediate and continuous measurement and increase costs, making them unrealistic for constant monitoring of the environment.

For these reasons, NTT has developed a compact and highly sensitive gas sensor system, which uses NTT's own μTAS together with ultraviolet spectroscopic technology. Even though the system's structure is simple, its sensitivity to minute quantities of gas is 1000 to 10,000 times greater than previous methods and it can perform continuous monitoring.

Recently, we have also achieved a detection sensitivity of 1 ppb or better for benzene in water by adding a liquid sample module based on newly developed bubbling and pervaporation methods [3] (**Fig. 5**). This R&D is described in detail in the Feature Article "Portable Sensor for Determining Benzene Concentration from Airborne/liquid Samples with High Accuracy" [11].

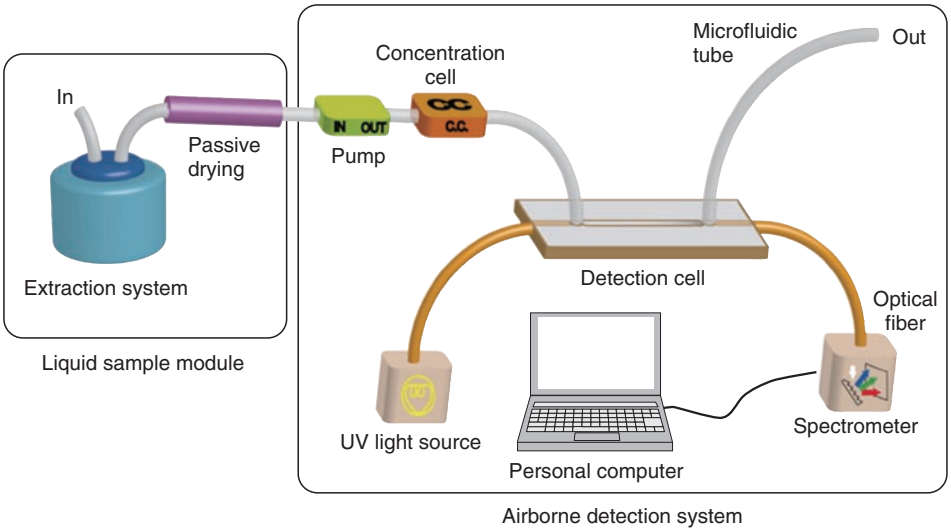

Fig. 5. Equipment for detecting benzene in water.

7. Conclusion

We have presented an overview of the work on imaging and sensing technology for safety that is underway in NTT. Efforts to improve the practicality and performance of the technology introduced here are continuing. Our objective is to achieve a safe and secure society by timely response to needs both within and outside NTT and by creating new technology.

References

[1] N. Shimizu, H. -J. Song, Y. Kado, T. Furuta, A. Wakatsuki, and Y. Muramoto, "Gas Detection Using Terahertz Waves," NTT Technical Review, Vol. 7, No. 3, 2009. https://www.ntt-review.jp/archive/ntttechnical.php?contents=ntr200903sf7.html

[2] K. Ajito, Y. Ueno, T. Haga, and N. Kukutsu, "Terahertz Spectroscopy Technology for Molecular Networks," NTT Technical Review, Vol. 7, No. 3, 2009. https://www.ntt-review.jp/archive/ntttechnical.php?contents=ntr200903sf6.html

[3] S. Camou, A. Shimizu, T. Horiuchi, and T. Haga, "Ppb-Level Detection of Benzene Diluted in Water with Portable Device Based on Bubbling Extraction and UV Spectroscopy," Sens. and Act. B, Vol. 32, No 2, pp. 601–607, 2008.

[4] S. Kaneko, S. Oka, and N. Matsumiya, "Detection of Cracks in Concrete Structures from Digital Camera Images," NTT Technical Review, Vol. 10, No. 2, 2012. https://www.ntt-review.jp/archive/ntttechnical.php?contents=ntr201202fa3.html

[5] H. Togo, T. Kojima, S. Mochizuki, and N. Kukutsu, "Millimeter-wave Imaging for Detecting Surface Cracks on Concrete Pole Covered with Bill-posting Prevention Sheet," NTT Technical Review, Vol. 10, No. 2, 2012. https://www.ntt-review.jp/archive/ntttechnical.php?contents=ntr201202fa2.html

[6] M. Tonouchi, "Cutting-edge Terahertz Technology," Nature Photonics, Vol. 1, No. 2, pp. 97–105, 2007.

[7] H. Ito, T. Nagatsuma, A. Hirata, T. Minotani, A. Sasaki, Y. Hirota, and T. Ishibashi, "High-power Photonic Millimetre Wave Generation at 100 GHz Using Matching-circuit-integrated Uni-traveling-carrier Photodiodes," Proc. of IEE Optoelectronics, Vol. 150, No. 2, pp. 138–142, 2003.

[8] A. Wakatsuki, Y. Muramoto, and T. Ishibashi, "Development of Terahertz-wave Photomixer Module Using a Uni-travelling-carrier Photodiode," NTT Technical Review, Vol. 10, No. 2, 2012. https://www.ntt-review.jp/archive/ntttechnical.php?contents=ntr201202fa5.html

[9] N. Shimizu, N. Kukutsu, A. Wakatsuki, and Y. Muramoto, "Remote Detection of Hazardous Gases in Full-scale Simulated Fire by Using Terahertz Electromagnetic Waves," NTT Technical Review, Vol. 10, No. 2, 2012. https://www.ntt-review.jp/archive/ntttechnical.php?contents=ntr201202fa4.html

[10] K. Ajito, Y. Ueno, and H. -J. Song, "Visualization of Pharmaceutical Drug Molecules by Terahertz Chemical Imaging," NTT Technical Review, Vol. 10, No. 2, 2012. https://www.ntt-review.jp/archive/ntttechnical.php?contents=ntr201202fa6.html

[11] S. Camou, E. Tamechika, and T. Horiuchi, "Portable Sensor for Determining Benzene Concentration from Airborne/liquid Samples with High Accuracy," NTT Technical Review, Vol. 10, No. 2, 2012. https://www.ntt-review.jp/archive/ntttechnical.php?contents=ntr201202fa7.html

Kimihisa Aihara
Director, Smart Devices Laboratory, NTT Microsystem Integration Laboratories.

He received the B.E. degree in electronics from Keio University, Kanagawa, in 1984. He joined Nippon Telegraph and Telephone Public Corporation (now NTT) in 1984. He is currently responsible for ubiquitous communications appliance technologies at NTT Microsystem Integration Laboratories. He is leading R&D projects on sub-terahertz-wave wireless communications, ultralow-power network appliances and electrical near-field communication for human area networks. He is a member of IEEE and the Institute of Electronics, Information and Communication Engineers (IEICE).

Naoya Kukutsu
Senior Research Engineer, Supervisor, Group Leader, Smart Devices Laboratory, NTT Microsystem Integration Laboratories.

He received the B.E., M.E., and D.E. degrees in electrical engineering from Hokkaido University in 1986, 1988, and 1991, respectively. His D.E. dissertation described research for a time-domain electromagnetic wave numerical analysis method. In 1991, he joined NTT Applied Electronics Laboratories in Musashino. His current research involves millimeter-wave and terahertz-wave transmission, as well as imaging systems. He is a member of the IEEE MTT and COM Societies and IEICE.

Millimeter-wave Imaging for Detecting Surface Cracks on Concrete Pole Covered with Bill-posting Prevention Sheet

Hiroyoshi Togo[†], *Takafumi Kojima, Shoji Mochizuki, and Naoya Kukutsu*

Abstract

In this article, we introduce millimeter-wave imaging technology for detecting submillimeter-wide cracks under a bill-posting prevention sheet on a concrete telegraph pole.

1. Introduction

NTT expends much effort in the long-term maintenance and management of the communication network to provide safe and secure communication services to customers throughout the country. Concrete telegraph poles, which are perhaps the most familiar of those facilities to most of us, are susceptible to physical damage, so a high degree of structural integrity is required. Concrete poles and other structures degrade over time; therefore, integrity maintenance requires periodic inspections so that degraded structures can be repaired. Since NTT owns more than ten million poles, such inspection is an every-day job for a large number of workers.

Concrete poles carry cables, transformers, and other equipment that produces an unbalanced load on the structure over many years. The resulting bending stress produces fatigue cracking on the pole surface. When such cracking penetrates as far as the rebar inside the pole, rainwater may enter and cause corrosion that can lead to the rebar breaking. The steel rebar, which is strong in tension, is vital to balance the concrete, which is strong in compression but weak in tension, so broken rebar reduces the integrity of a concrete pole. Considering this degradation mechanism, we focused on the initial stage of degradation, which is the appearance of cracks on the concrete surface. NTT has experimentally verified that submillimeter-wide surface cracks have a high probability of reaching the rebar, so early discovery of the initial degradation is considered to be the best approach to structural integrity maintenance. Therefore, careful visual inspection of the pole surface is performed.

NTT Access Network Service Systems Laboratories is developing a new technique to replace human visual inspection by using software to automatically detect cracks from images acquired by a digital camera. More details of that technique are given in the Feature Article “Detection of Cracks in Concrete Structures from Digital Camera Images,” in this issue [1].

To prevent unauthorized posting of advertisements on concrete poles, 2-mm-thick sheets of textured polyvinyl chloride (bill-posting prevention sheets) are bonded to the poles with acrylic resin in the region within reach by hand (**Fig. 1**). Exposing the covered surface for a visual inspection would require significant work to strip off the sheet and then replace it with a new one after the inspection. Since that would not be economically feasible, we conducted research and development (R&D) of a nondestructive

† NTT Microsystem Integration Laboratories
Atsugi-shi, 243-0198 Japan

Fig. 1. Bill-posting prevention sheet on a concrete pole.

inspection technique that allows observation of the condition of the pole surface without the need to remove the bill-posting prevention sheet.

2. Nondestructive inspection technology

Methods for seeing through the covering material to observe the condition of the surface beneath it are classified by the physical phenomena that are utilized. In particular, methods that use x-rays, ultrasonic waves, or microwaves have been applied in various fields.

X-rays are a form of ionizing radiation that have high transmittance for materials other than water and heavy metals and allow imaging with micrometer-order spatial resolution. They are applied for medical purposes such as 3D imaging of internal organs and bones, but since they are harmful to humans, exposure levels must be carefully controlled: this would be a safety problem for workers using x-rays to inspect multiple concrete poles every day. Another problem is that practical x-ray imaging equipment is based on transmission, so it should really have a separate transmitter and receiver; however, for work sites with limited work space, reflection-based imaging equipment can be used.

Ultrasonic waves are elastic waves[*1] that have almost no effect on the human body and have high transmittance and millimeter-order spatial resolution for reflection-based imaging. They are therefore used for medical three-dimensional imaging of fetuses etc., but the procedure requires the application of grease between the ultrasonic wave transceiver and the object to be observed for efficient sound wave transmission. The expense of applying and removing grease would be a problem of the inspection of a huge number of poles.

Microwaves are electromagnetic waves that have high transmittance and centimeter-order spatial resolution inside concrete, so they are used to inspect rebar. However, this technique does not provide the submillimeter-order spatial resolution required for crack detection, so imaging performance remains a problem.

3. Millimeter-wave imaging technology

To overcome the problems of safety, economy, and imaging performance, we took up the difficult R&D challenge of using millimeter waves, which are electromagnetic waves of higher frequencies than micrometer waves, to develop improved imaging technology. The millimeter-wave band includes frequencies from 30 GHz to 300 GHz, but the frequencies specified by the Radio Law for radar use (imaging is also one use of radar) range only from 76 GHz to 77 GHz (the band allocated to millimeter-wave radar). Considering the near future, the allocation of millimeter-wave radar band frequencies for inspection purposes is being studied. The main problems of concern in developing millimeter-wave radar technology for detecting cracks in concrete poles under bill-posting prevention sheets are 1) the transmittance of the plastic sheet, 2) submillimeter spatial resolution, and 3) the ease of equipment operation.

In the band allocated for millimeter-wave radar, the relative permittivity of polyvinyl chloride is about 3 and the dielectric tangent is about 0.01, so if we assume a planar wave incident on a 4-mm-thick infinite plane, the attenuation due to reflection and propagation loss is low, about -10 dB, so transmittance is not a significant problem for equipment design. There is concern, however, that the texture of the bill-posting prevention sheet may have a greater effect on attenuation than the sheet's material properties because of wave scattering at the surface.

Another factor is that the width of the cracks to be detected is less than 1/10 the wavelength of the band allocated to millimeter-wave radar, so considering the radar cross-section area, the back scattering will be less than -30 dB relative to the power irradiating the

*1 Elastic wave: Wave of deformation in an elastic body.

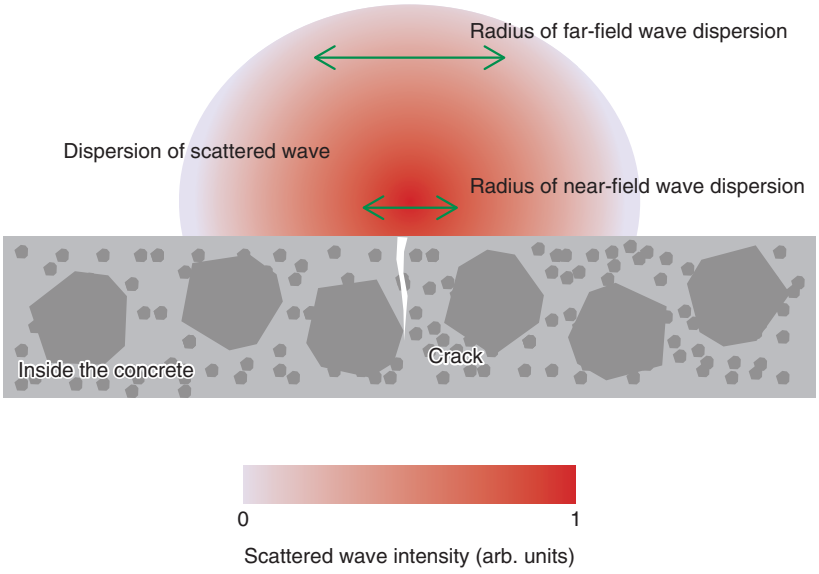

Fig. 2. Dispersion of wave-scattering from a crack.

surface. On the basis of the above estimates, we are investigating an equipment design in which the irradiation power of the millimeter-wave radiation is set to -50 dB to pass through the bill-posting prevention sheet to reach the crack and then pass back through the sheet again as back-scattering.

Because the minimum beam diameter obtainable by focusing with a quasi-optical system using a lens is limited by diffraction, the beam width is limited to approximately the wavelength. The spatial resolution is therefore about half the wavelength, which means that it is difficult to detect submillimeter-wide cracks using the approximately 4-mm wavelength of the band allocated to millimeter-wave radar. For that reason, we have been trying to improve the spatial resolution by detecting near-field scattering. The concept, as shown in **Fig. 2**, is that the spatial resolution can be improved because the waves scattered from the crack, which can be regarded as a minute point in a cross-section that includes the crack width direction and the crack depth direction, are spherical waves[*2]. The dispersion of the scattered waves is thus small in the near field. Detecting near-field scattering with submillimeter-order spatial resolution requires the use of an antenna whose aperture is equivalent to the width of the scattered waves at the detection height. We are therefore investigating aperture design at the antenna placement height with consideration given to operability.

Inspecting all of the concrete telegraph poles in the entire country for structural integrity requires highly efficient work. The shortest imaging time could be achieved by covering the entire bill-posting prevention sheet with the antenna for detecting near-field scattering that is needed in the detection of submillimeter-wide cracks, but it is difficult to arrange antenna elements at submillimeter intervals in the crack width direction. Even if the elements were arranged at millimeter intervals, since the bill-posting prevention sheet is about 1.5 m long in the vertical direction, the number of antenna and millimeter-wave transmitter and receiver components would be huge and the equipment cost would be uneconomical. The equipment would also be large, which would reduce its portability. To maintain economy and portability, we considered a method in which ten antennas are arranged in a one-dimensional array in the crack length direction and the array is scanned in the crack width direction. Spatial resolution in the crack width direction is maintained by detecting scattered waves at submillimeter intervals. The equipment can perform multiple scans in the crack length direction in order to image the entire surface.

*2 Spherical wave: Wave motion that emanates from a single point in a three-dimensional isotropic medium or that converges to a single point.

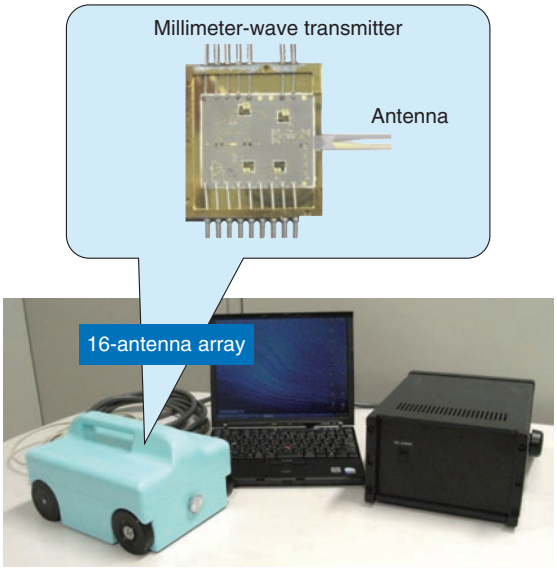

Fig. 3. CP Scan equipment.

Fig. 4. Schematic illustration of CP Scan in use.

4. Concrete pole inspection equipment

On the basis of the design policy described above, we constructed portable equipment (CP Scan) for detecting cracks in concrete poles under bill-posting prevention sheets (**Fig. 3**). Sixteen intensity-phase detection modules having tapered slot antennas are arranged in a one-dimensional array. A signal from the module is input to the baseband circuit at submillimeter scanning intervals in sync with a signal from an encoder attached to the wheels of the unit: in this way, the condition of the concrete pole surface is imaged. The case containing the module, encoder, and baseband circuit weighs less than 4.1 kg and can be held in one hand for scanning. The entire system, including the power supply and personal computer, weighs less than 10 kg and can be carried by a single person. The 16 modules can image an 8-cm-wide path in a single scan, and one or two workers can inspect a pole in about three minutes by making five or six scans to completely image the entire region of the bill-posting prevention sheet (**Fig. 4**).

5. Feasibility of submillimeter-wide crack detection

To test the practicality of the CP Scan, a bill-posting prevention sheet was attached to a concrete pole that had been removed for renovation (**Fig. 5**) and the CP Scan was used to inspect this area. The pole had cracks ranging in width from 0.3 mm to 0.15 mm. Although this preliminary experiment was suitable for confirming the method's principle, the attached bill-posting prevention sheet was not bonded to the pole. The scanning rate was 120 mm/s with data being acquired at intervals of 0.2 mm in the scanning direction. That rate will allow one concrete pole to be inspected in about three minutes. A millimeter-wave image was obtained after three scans (**Fig. 6**). Although the equipment must be calibrated, the imaging only requires the equipment to be kept tightly against the pole during the scan, so the operation is simple.

To allow a single person to perform the inspection, as shown in Fig. 5, the power supply and personal computer parts of the system must be small and light, and image processing is essential for automatic crack detection from the acquired images. Therefore, NTT Access System Laboratories is currently developing an algorithm suitable for millimeter-wave image analysis.

These experiments used the Crack Scan automatic crack detection software that was subject to hard disclosure commissioning to Airec Engineering Corporation in 2008 for evaluation of the detection characteristics. The red solid lines in the bottom row of Fig. 6 indicate cracks detected by the Crack Scan automatic detection algorithm, confirming that 0.15-mm-wide cracks can be detected. These results open up the prospect of developing portable equipment

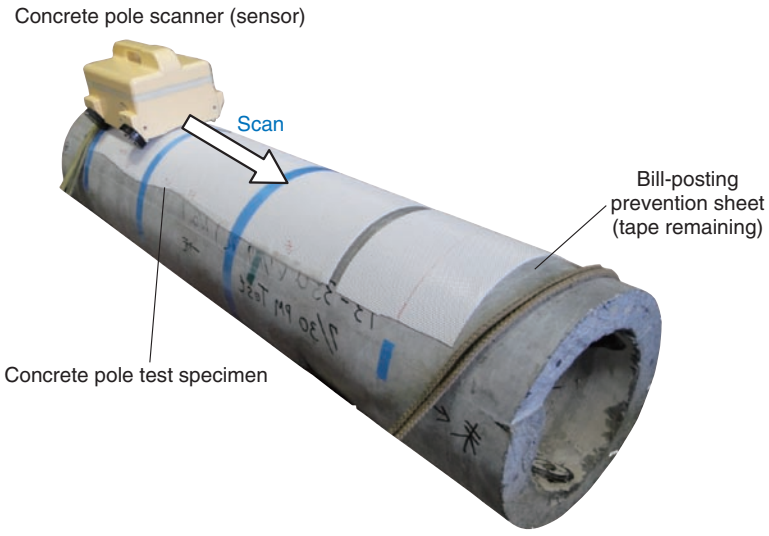

Fig. 5. Experimental setup.

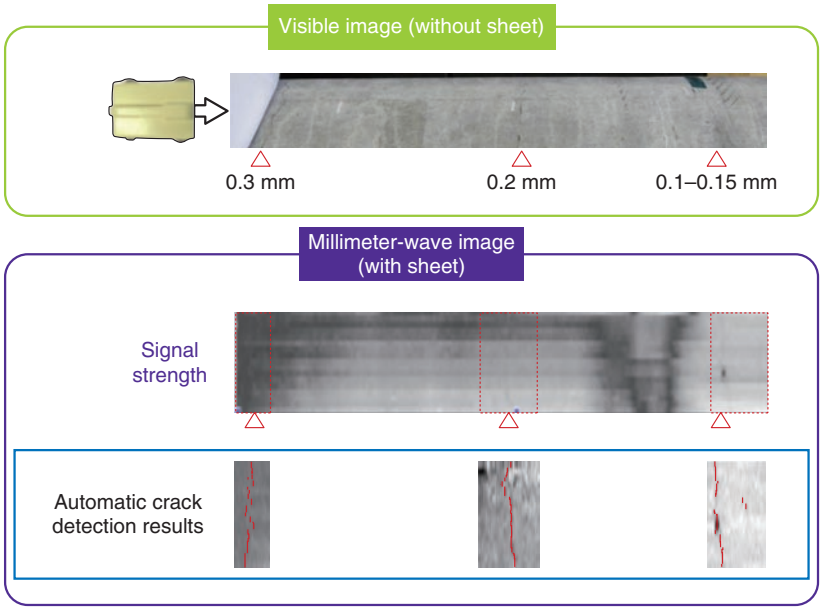

Fig. 6. Results of crack detection in test specimen.

that can detect cracks that are at least 0.15 mm wide with a scanning time of about three minutes per pole.

6. Future plans

In future work, we will test the system's practicality on actual poles with bill-posting prevention sheets bonded to them and evaluate the detection performance with our automatic crack detection software for millimeter-wave images of concrete poles. We will continue conducting R&D that will have wide applicability with highest priority on ease of operation and higher inspection efficiency while achieving

practical detection performance suitable for equipment that can be used in actual concrete pole inspection work.

References

[1] S. Kaneko, S. Oka, and N. Matsumiya, "Detection of Cracks in Concrete Structures from Digital Camera Images," NTT Technical Review, Vol. 10, No. 2, 2012.
https://www.ntt-review.jp/archive/ntttechnical.php?contents=ntr201202fa3.html

[2] S. Oka, S. Mochizuki, H. Togo, and N. Kukutsu, "Inspection of Concrete Structures Using Millimeter-wave Imaging Technology," NTT Technical Review, Vol. 7, No. 3, 2009.
https://www.ntt-review.jp/archive/ntttechnical.php?contents=ntr200903sf4.html

Hiroyoshi Togo

Senior Research Engineer, NTT Microsystem Integration Laboratories.

He received the M.Sc. and Ph.D. degrees in applied physics and electronic engineering from the University of Tsukuba, Ibaraki, in 1996 and 2010, respectively. He joined NTT Musashino Opto-electronics Laboratories in 1996. From 1996 to 2001, he was engaged in the development of a thermo-capillary waveguide-based optical switch and from 2001 to 2002, he endeavored to commercialize it for NTT Electronics Inc. Since 2002, he has been researching ultra-wideband impulse radio systems using photonic techniques and millimeter-wave tomography with electro-optic probing. He is a member of the IEEE Photonics, Antenna and Propagation, and Microwave Theory and Techniques Society and the Institute of Electronics, Information and Communication Engineers (IEICE). He received the 2006 Asia Pacific Microwave Photonics Conference AP-MWP Award and the 2010 European Conference on Antennas and Propagation Award.

Takafumi Kojima

Research Scientist, NTT Microsystem Integration Laboratories.

He received the B.S., M.S., and Ph.D. degrees in physics from Osaka Prefecture University in 2005, 2007, and 2010, respectively. During 2007–2010, he was engaged in R&D of terahertz superconductor-insulator-superconductor mixers at the National Astronomical Observatory of Japan, Tokyo. He joined NTT Microsystem Integration Laboratories in 2010 and is currently studying radar signal processing for millimeter imaging. He received the 27th JSAP (Japan Society of Applied Physics) Incentive Award for Excellent Presentation in 2009, the 14th Superconductivity Science and the Technology Award from the Society of Non-Traditional Technology in 2011. He is a member of IEEE, JSAP, and IEICE.

Shoji Mochizuki

Research Scientist, NTT Microsystem Integration Laboratories.

He received the B.E., M.E., and Ph.D. degrees in electrical and electronic engineering from Chuo University, Tokyo, in 2001, 2003, and 2005, respectively. He joined NTT Microsystem Integration Laboratories in 2005 and is currently working on R&D of millimeter-wave and microwave imaging. He received the 2004 International Union of Radio Science (URSI) Commission B Young Scientist Award. He is a member of IEEE and IEICE.

Naoya Kukutsu

Senior Research Engineer, Supervisor, Group Leader, Smart Devices Laboratory, NTT Microsystem Integration Laboratories.

He received the B.E., M.E., and D.E. degrees in electrical engineering from Hokkaido University in 1986, 1988, and 1991, respectively. His D.E. dissertation described research for a time-domain electromagnetic wave numerical analysis method. In 1991, he joined NTT Applied Electronics Laboratories in Musashino. His current research involves millimeter-wave and terahertz-wave transmission, as well as imaging systems. He is a member of the IEEE MTT and COM Societies and IEICE.

Detection of Cracks in Concrete Structures from Digital Camera Images

Suguru Kaneko†, Soichi Oka, and Naoki Matsumiya

Abstract

In this article, we introduce an image processing technique for detecting fine cracks in concrete poles by examining remotely acquired photographs.

1. Introduction

NTT has many concrete structures as communication infrastructure facilities and it performs periodic inspections of them for safety maintenance and management. Those structures include a particularly large number of concrete poles, so efficient inspection is essential.

The on-site inspection for cracks in the concrete surface of a concrete pole is meticulous because cracks allow rainwater to enter and corrode the rebar inside, which reduces the strength of the structures. Current crack inspection methods mainly involve human visual inspection, but it is difficult for workers to maintain concentration over a long period of work, and even skilled inspectors can overlook fine cracks. In particular, when inspecting concrete poles for cracks, workers must use binoculars rather than the naked eye and continuously focus on locations that can be ten meters high or higher. This is fatiguing, which also makes it difficult for the workers to maintain concentration. Furthermore, the number of inspectors is decreasing year by year and this has increased the workload per worker.

These circumstances necessitate increased efficiency in crack inspection through automation of on-site inspections. From the viewpoint of ease of handling and operation of equipment, remote photography of structures with digital cameras and automatic crack detection from the obtained images by software is an effective approach. In this article, we describe the most recent image processing algorithms that have overcome technical problems for practical use.

† NTT Access Network Service Systems Laboratories
Tsukuba-shi, 305-0805 Japan

2. Difficulty of crack detection by image processing techniques

Algorithms for automatic detection of cracks from images of concrete surfaces have already been proposed, but the existing methods have problems in terms of practicality. In efforts to detect cracks by image processing, cracks are generally defined using edge features, regardless of the algorithm used. Cracks are represented as sharp changes in gray-scale values between edges and adjoining pixels that form an outline and appear in images as darkened lines. Thus, edges are the unique feature that indicates cracks. These algorithms are effective for images that include only concrete surfaces, but they do not work well when the image also includes extraneous obstacles. The reason for the poor performance in practice is that images of actual on-site concrete structures often include obstacles such as windows and sashes in the case of buildings and cables or foot pegs in the case of concrete poles. The edges formed by the outlines of such obstacles can be mistaken for cracks. An example of results produced by commercial crack detection software is presented in **Fig. 1**. The pixels colored red indicate areas judged by the software to be cracks, and we can see that the background, belts, plates, and other edges were erroneously detected as

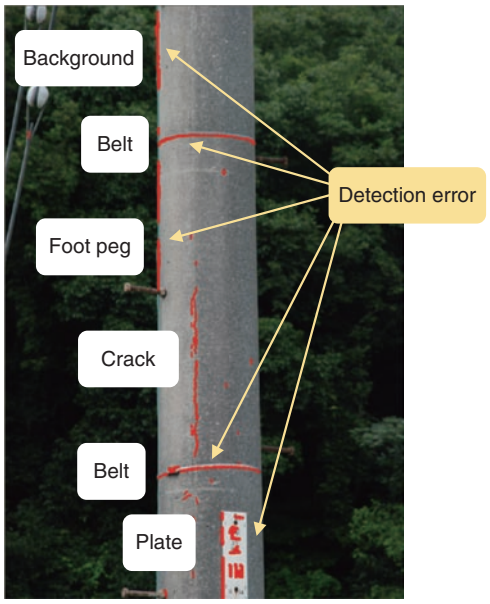

Fig. 1. Results from commercial crack detection software.

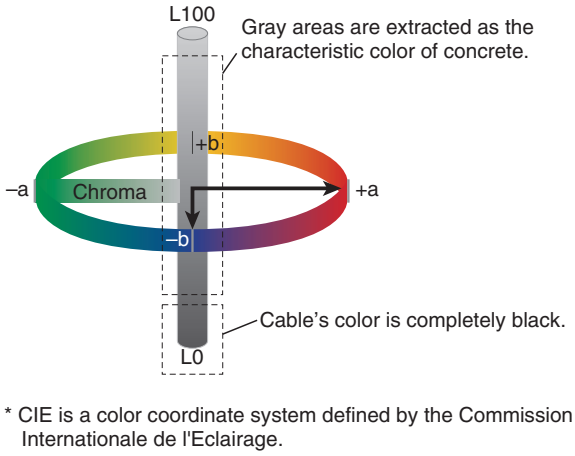

* CIE is a color coordinate system defined by the Commission Internationale de l'Eclairage.

Fig. 2. CIE Lab color system*.

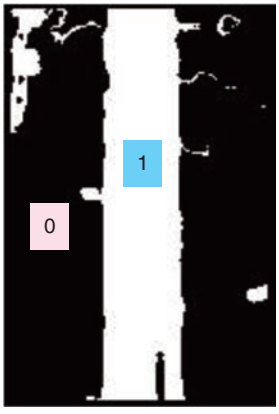

Fig. 3. Color classification results.

cracks. To overcome this problem, it is necessary to eliminate such obstacles from the image before performing the crack detection processing. However, it is not easy to obtain a highly accurate solution with current pattern recognition techniques because of the infinite variety in obstacle shapes. Accordingly, extracting only the cracks from images that include such obstacles has been very difficult.

3. Obstacle removal algorithm

Because various obstacles exist at the site of actual facilities, as mentioned above, it is not easy to eliminate obstacles by defining their shapes and creating an algorithm to remove them directly. Therefore, with our algorithm, we chose to take the opposite approach of indirect obstacle removal. The indirect approach involves extracting the pole's concrete surface and inverting the results. We explain the main points of the algorithm below.

First, we extract from the input image pixels that seem to represent concrete surface. Because the concrete surface is generally gray, we can use a color system such as the one shown in **Fig. 2** to represent color chrominance numerically and extract the gray pixels, which have low chrominance values. In the color classification results (**Fig. 3**), the pixels that are nearly gray are made white and pixels that are not close to gray are made black. This image has a green forest as the background, so color classification can be used to identify the rough outline of the concrete pole, but if the image contains a gray structure, the concrete pole can be identified by the amount of texture. It was therefore necessary to supplement the color information with texture information as explained below in order to extract concrete pole surfaces from various types of images with greater certainty.

The concrete surface, which consists of cement and fine grains of sand, has a characteristically rougher texture pattern than other materials usually found in images. We know the pole's roughness pattern and can thus distinguish concrete pole from other gray objects. This surface roughness pattern is referred to as texture in image analysis terminology, and it is

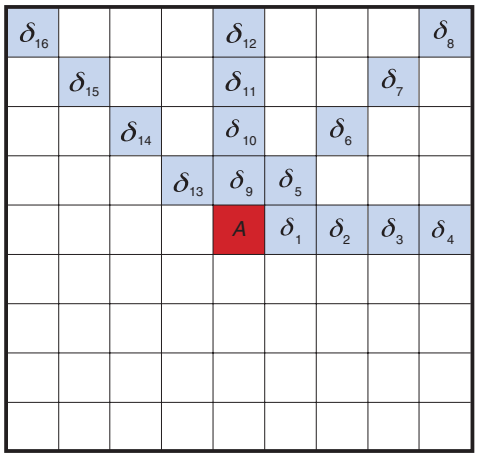

Fig. 4. Area for texture calculations.

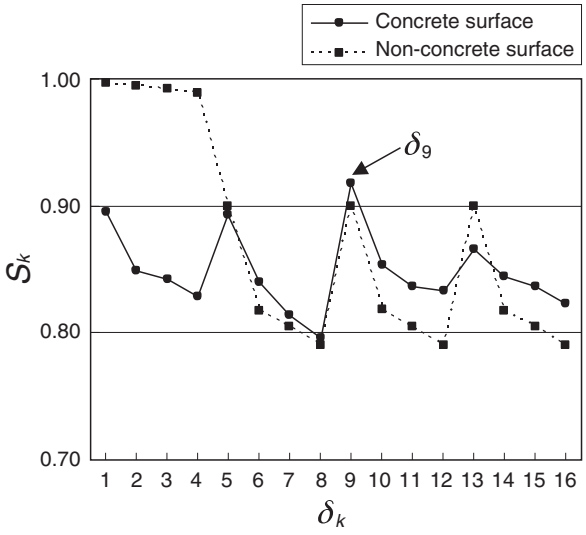

Fig. 5. Comparison of texture for concrete and non-concrete surfaces.

used in judging materials. In our algorithm, we obtain a numerical value for the texture feature S of the concrete surface by calculating the homogeneity of 16 pixels in a pattern around a particular pixel, such as the light blue pixel formation (δ_1 to δ_{16}) around the red pixel A in **Fig. 4**. The specific method used to calculate the texture feature is described in Ref. [1].

Calculating the homogeneity for the 16 pixels produces 16 texture values, Sk (k=1, 2, …, 16). The relation between δ and S is plotted in **Fig. 5**, where the solid line represents the calculated results for the concrete surface and the broken line represents the

Fig. 6. Obstacle removal results.

calculated results for non-concrete surfaces. As we can see from the figure, the shape of the graph differs greatly for concrete and non-concrete surfaces. It is therefore possible to determine whether or not a pixel is part of a concrete surface by comparing its graph with stored reference graphs for concrete surface texture features.

In the final step, the conjunction of the color classification results and texture classification results is taken. If either result does not indicate a concrete pixel, then that pixel is judged to be not a concrete pixel and obstacle removal is completed. Obstacle removal results are shown in **Fig. 6**, where the transparent red areas show the obstacle pixels. We can see that the background, bands, plates, and foot pegs, etc. have been removed.

4. Crack detection algorithm

After obstacle removal, cracks are extracted from the concrete surface areas of the image. This algorithm applies a method that emulates human neural circuitry with a neural network.

The areas of concrete surface in the image after obstacle removal are partitioned into small rectangles, and a search for cracks is performed. The crack edge features are extracted, and cracks are detected by the neural network. With this algorithm, we emulate the

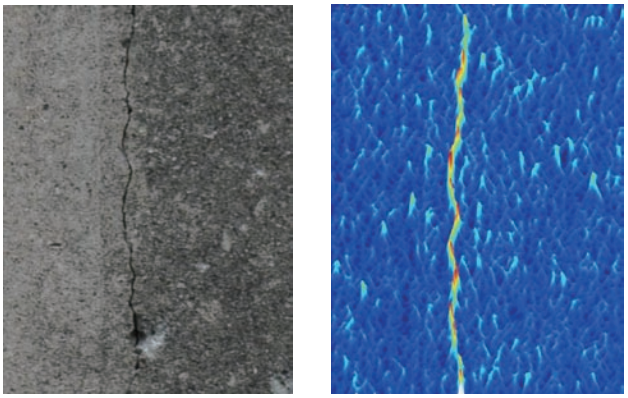

Fig. 7. Crack image (left) and extracted edge feature (right).

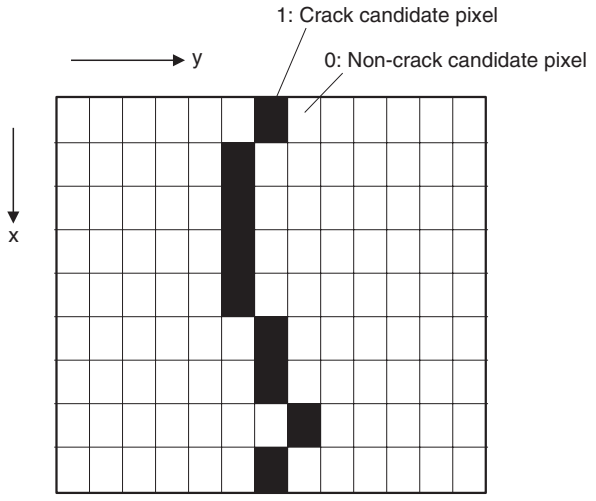

Fig. 8. Problem representation using a two-dimensional array of neurons.

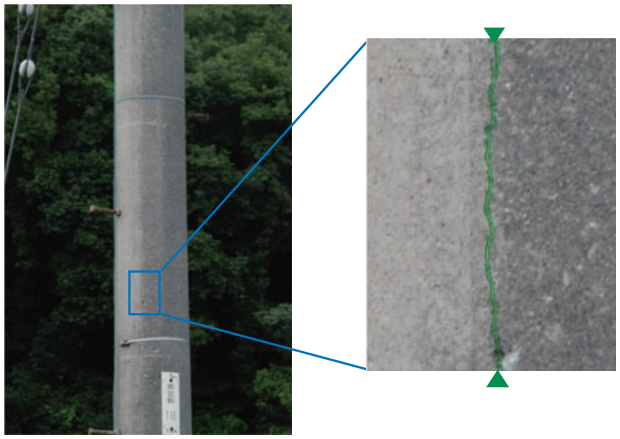

Fig. 9. Crack detection results.

mechanism with which we see objects with our eyes, and implement a crack line detection function that works in exactly the same way as the human eye and brain do. An original crack image and the extracted edge feature are shown in **Fig. 7**. The crack image is 300 × 300 pixels and the edge filter is 26 × 18 pixels.

Next, the neural network extracts the crack shape from the obtained edge feature. As shown in **Fig. 8**, the problem is represented as a two-dimensional array of neurons that is the same size as the edge image, and the neural network searches for edges that conform to the crack shape. The specific method of using the neural network to construct the expression of behavior is described in Ref. [2]. In the crack detection results (**Fig. 9**), the neurons (green pixels) are seen to correspond to the crack.

5. Concluding remarks

NTT Group companies are going to apply the crack detection technique described here to concrete pole inspection, and the technique is expected to play a useful role in the maintenance and management of safe facilities. Furthermore, NTT manages many concrete structures that require periodic inspection besides concrete poles, so we would like to improve this technique to enable it to meet the crack inspection needs of other structures.

References

[1] Ed. by M. Takagi, "Image Analysis Handbook," New Edition, University of Tokyo Press, 2004.
[2] S. Oka, S. Mochizuki, H. Togo, and N. Kukutsu, "A Neural Network Algorithm for Detecting Invisible Concrete Surface Cracks in Near-field Millimeter-wave Images," Proc. of IEEE International Conference on Systems, Man, and Cybernetics (SMC2009), San Antonio, TX, USA, 2009

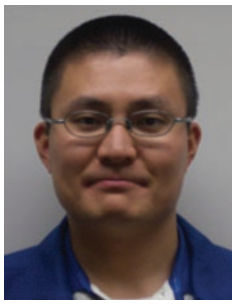

Suguru Kaneko
Engineer, Civil System Project, NTT Access Network Service Systems Laboratories.
He received the B.E. degree in quantum and electronic engineering from Tsukuba University, Tsukuba, in 2002 and the M.E. degree in physical electronics from Tokyo Institute of Technology, Tokyo, in 2003. He joined NTT EAST in 2003 and moved to NTT Access Network Service Systems Laboratories in 2008. He is currently engaged in research on maintenance technology for civil infrastructure facilities.

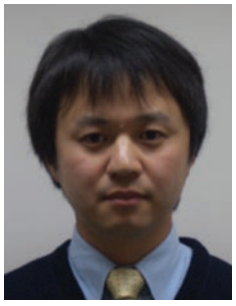

Soichi Oka
Senior Research Engineer, NTT Access Network Service Systems Laboratories.
He received the B.E. degree in environmental information and the M.E. and Ph.D. degrees in media and governance from Keio University, Kanagawa, in 1996, 1998, and 2001, respectively. During 2002–2003, he was engaged in R&D of evanescent microwave imaging at Wright Patterson Air Force Research Laboratories and the University of Cincinnati in Ohio, USA. Since joining NTT in 2004, he has been engaged in R&D of nondestructive inspection systems.

Naoki Matsumiya
Senior Chief Engineer, NTT Access Network Service Systems Laboratories.
He received the B.E. degree in environmental information and the M.E. degree in civil engineering from Nagoya University, Aichi, in 1985 and 1987, respectively. He joined NTT in 1987 and worked in the Access Network Service Systems Laboratories from 1988 to 1992. He is currently engaged in R&D of management and maintenance technology for civil infrastructure facilities.

Remote Detection of Hazardous Gases in Full-scale Simulated Fire by Using Terahertz Electromagnetic Waves

Naofumi Shimizu†, *Naoya Kukutsu, Atsushi Wakatsuki, and Yoshifumi Muramoto*

Abstract

This article describes a prototype spectroscopic sensing system that we have developed for detecting hazardous gases at the scene of a fire from a distance. First, the system's terahertz signal generator and receiver are briefly described. Then, sub-terahertz-band absorption spectra of smoke generated from heated nylon fabric are explained. Finally, a performance test of the developed sensing system carried out in a full-scale simulated fire is presented.

1. Introduction

Our research and development (R&D) activities for detecting hazardous gases from a distance with terahertz electromagnetic waves were previously reported in NTT Technical Review in 2009 [1]. The research began in 2006 and continued under commission from the National Institute of Information and Communication Technology (NICT). At the end of 2010, the last year of the commission, we succeeded in detecting hazardous gases from a distance in a full-scale simulated fire by using a prototype of the terahertz spectroscopic sensing system [2]. In the following sections, we first outline the basic concept of the remote spectroscopic sensing system. We then describe the terahertz signal generator and receiver used in the system. Finally, we present the results of some experiments done with the system: small-scale experiments using a gas cell and large-scale experiments with a full-scale simulated fire.

2. Sensing system

The operation of the remote gas sensing system is illustrated schematically in **Fig. 1**. Carbon monoxide, hydrogen cyanide, and other hazardous gases generated by fires have characteristic absorption spectra in the terahertz band. The remote spectroscopic sensing system determines whether or not a hazardous gas is present around the target by sending terahertz electromagnetic waves to the target and analyzing the spectrum of the waves returned from the target. The system requires a terahertz transmitter and terahertz receiver with a wide operating frequency range. To meet the requirement, we used a photomixing technique to generate the terahertz electromagnetic waves. The optical signal generator comprises three laser sources that emit light waves in the 1.5-μm band (**Fig. 2**). One of the lasers is a tunable-wavelength laser source (TLS); the other two are fixed-wavelength laser sources (FLSs). The signal generated by the TLS is first split and the resulting signals are mixed with the outputs of both FLS1 and FLS2 to generate optical beat signals. Those two optical beat signals are converted into terahertz electromagnetic waves by a uni-traveling carrier photodiode (UTC-PD) module [3]. The FLS wavelengths are set so that there is a 350-MHz frequency difference between them. As a result, the frequency difference of the two generated terahertz electromagnetic waves is 350 MHz and is independent of the wavelength of the

† NTT Microsystem Integration Laboratories
Atsugi-shi, 243-0198 Japan

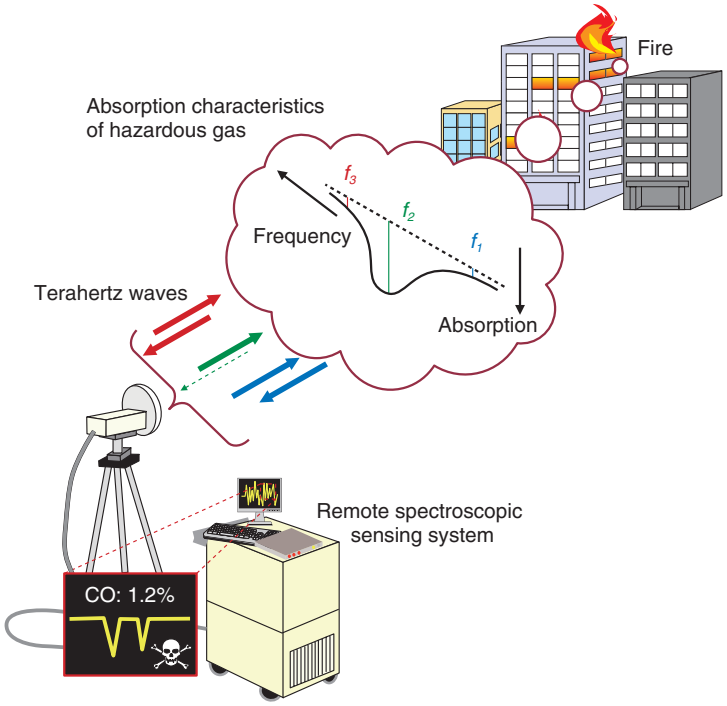

Fig. 1. Operating principle of remote spectroscopic sensing system.

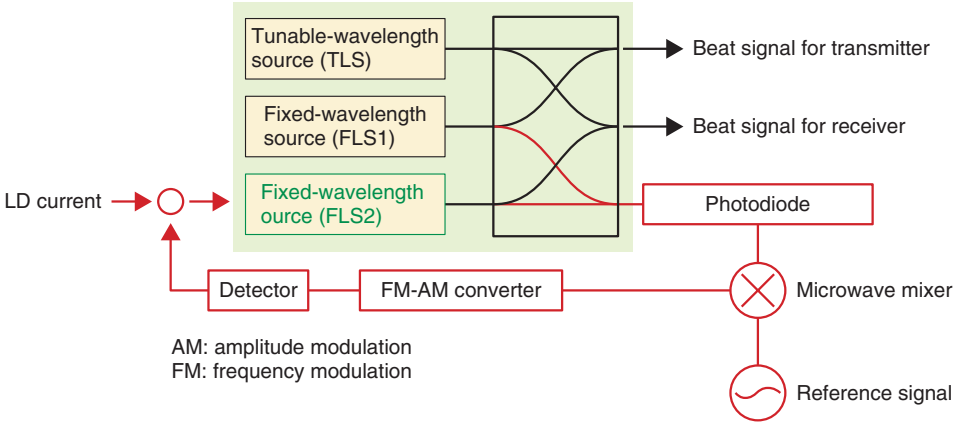

Fig. 2. Optical signal generator.

TLS. When we use the two terahertz electromagnetic waves as sensing waves and as the local oscillator signal of the heterodyne receiver, the frequency of the heterodyne receiver's intermediate frequency signal can be made constant at 350 MHz. This means that we do not have to widen the bandwidth of the intermediate frequency circuit needlessly, even if we change the frequency of the terahertz electromagnetic waves very rapidly. Consequently, we can keep the receiver's noise level very low.

Furthermore, small proportions of the two FLS outputs are extracted and coupled, and their beat signal is obtained. This beat signal is mixed with the reference signal and their frequency error is extracted. This error is fed back as the driving condition of FLS2. Thus, the frequency difference of the FLSs is

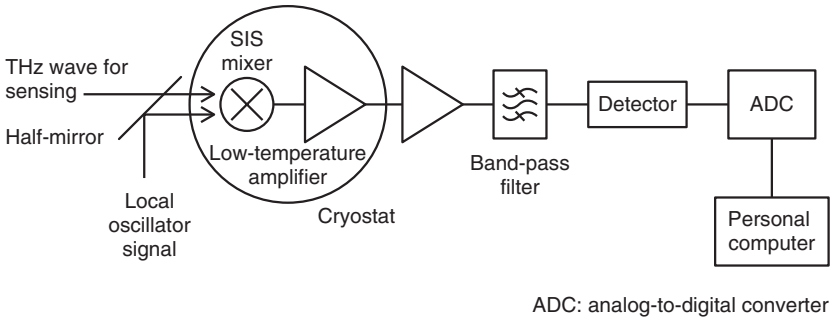

Fig. 3. Receiver block diagram.

locked. In this study, the FLS wavelengths were set to near 1548.959 nm, and the TLS wavelength was swept between 1547.3631 nm and 1544.971 nm in less than 1 s. The corresponding frequency sweep was from 200 GHz to 500 GHz. Details of the UTC-PD modules used in this study are given in another Feature Article in this issue [3].

A block diagram of the receiver is shown in **Fig. 3**. The mixer that we used for heterodyne detection was the superconductor-insulator-superconductor tunneling (SIS) mixer developed by the National Institute of Advanced Industrial Science and Technology [4]. The mixer and the low-temperature amplifier that amplifies the intermediate frequency signal output are inside a mechanical cooler and maintained at the temperature of liquid helium. The terahertz signal used for sensing is combined with the local oscillator signal by a coupler placed just in front of the receiver and then fed to the SIS mixer. The received sensing waves are converted to an intermediate frequency signal by the SIS mixer. After boosting by the low-temperature amplifier, the out-of-band noise is removed and the signal is converted to a voltage signal that is proportional to the signal strength. The voltage signal is acquired by a personal computer via an analog-to-digital converter connected to the detector's output. The signal is combined with the wavelength data to obtain the spectrum. An overall view of a remote spectroscopic sensing system that comprises the terahertz signal generator, receiver, and optics is shown in Ref. [5]. We performed all of the experiments described below in electromagnetically shielded areas.

3. Transmission spectrum of smoke

Smoke from heated nylon fabric was supplied via a heated pipe to a gas cell that was 1 m long and 10 cm in diameter. A photograph of the cell filled with the generated smoke is shown in **Fig. 4**. The smoke was so dense that it was impossible to see the wall on the other side of the cell. The smoke consisted of a large number of suspended particles with diameters of several micrometers. The wavelength of the terahertz waves used for sensing was about 1 mm, which is two or three orders of magnitude larger than the particles. Accordingly, the sensing waves were not scattered by the particles. That is, such a dense smoke is transparent to the sensing waves. Therefore, we could observe the characteristic absorption spectra of the gases in the smoke when we measured the smoke's absorption spectra with the developed terahertz electromagnetic waves generator and receiver. The results are shown in **Fig. 5**. At 240 s and 480 s after the nylon fabric began to be heated, absorption peaks were observed at 265 GHz, 355 GHz, and 444 GHz. Those peak frequencies agree well with the absorption frequencies of hydrogen cyanide molecules. A detailed

Fig. 4. Gas cell filled with smoke.

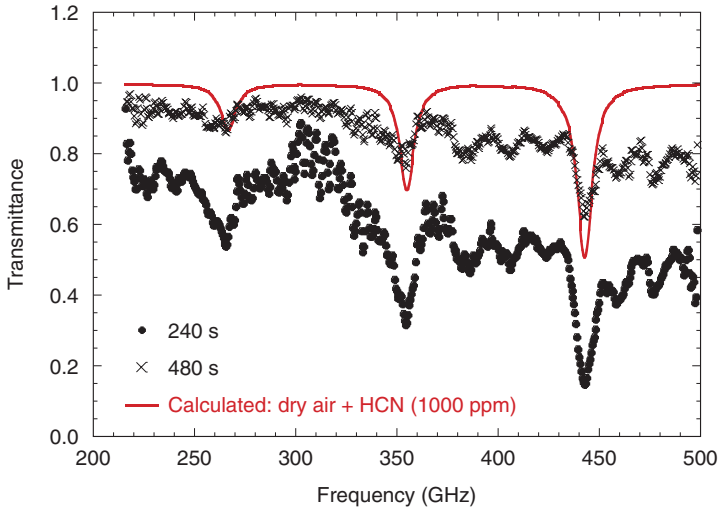

Fig. 5. Absorption spectra of smoke.

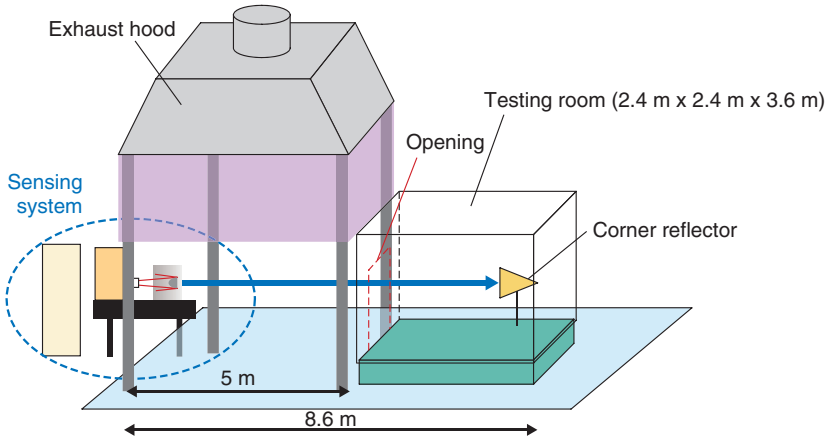

Fig. 6. Setup in the fire test hall.

analysis clarified that the spectrum included the absorption peaks of hydrogen cyanide, acetonitrile, and water [6]. Nylon is an organic polymer that contains amide bonds. Therefore, the observed spectra suggest that the nylon fabric burned incompletely in this experiment.

4. Gas detection in a full-scale fire

Next, we present the results of remote gas sensing experiments conducted in a full-scale simulated fire. The setup in the fire test hall at the Center for Fire Science and Technology at the Tokyo University of Science is illustrated in **Fig. 6**. We put urethane blocks in a testing room and ignited them. The testing room imitates a small room and its inside dimensions are 2.4 m wide, 3.6 m deep, and 2.4 m high. The testing room filled with smoke and gases generated by the fire within a minute after ignition. The remote spectroscopic sensing system was placed 5 m from the testing room and transmitted terahertz waves toward the room's opening. In this experiment, the terahertz waves were reflected by a metal corner reflector placed on the opposite side of the testing room facing the sensing system. Some of the returned terahertz waves were received by the remote

Fig. 7. Opening of the testing room seen from the sensing system.

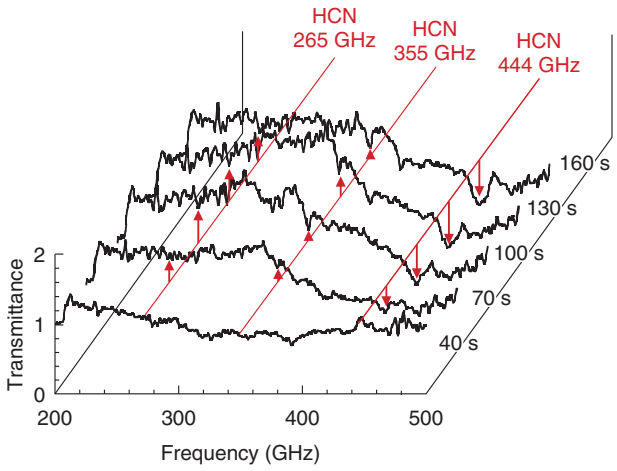

Fig. 8. Absorption spectra measured with the remote spectroscopic sensing system.

spectroscopic sensing system.

The room's opening as seen from behind the remote spectroscopic sensing system is shown in **Fig. 7**. The measured absorption spectra of the terahertz waves are shown in **Fig. 8**. Absorption peaks were clearly observed at 265 GHz, 355 GHz, and 444 GHz between 70 s and 160 s after ignition. Those frequencies are consistent with the absorption frequencies of hydrogen cyanide molecules. The average value of the hydrogen cyanide concentration estimated from the measured absorption intensity at a time between 100 s and 250 s was 890 ppm. In this experiment, the gas inside the testing room was sampled over the time period between 90 s to 300 s. Chemical analysis of the sampled gas revealed a hydrogen cyanide concentration of 640 ppm, which is consistent with the value obtained by the remote spectroscopic sensing system. These results show that the terahertz remote spectroscopic sensing system succeeded in realtime remote monitoring of hazardous gases generated by a fire.

The main purpose of the experiments reported here was to verify the basic operation of active remote spectroscopic sensing in the terahertz band. We therefore used an artificial metal corner reflector to reflect the terahertz electromagnetic waves effectively. However, this does not mean that such a reflector is always required in actual situations. For example, the intersections of three orthogonal planes at room corners or at a protruding wall also form corner-reflector structures. Such non-metallic corner reflector structures made by the wall's materials certainly exist on the interior and exterior walls of structures. We believe that terahertz electromagnetic waves of sufficient intensity can be returned when we irradiate such structures with terahertz electromagnetic waves. We have already confirmed that a corner reflector made of concrete panels effectively reflects terahertz waves.

5. Concluding remarks

We have reported on remote detection of hydrogen cyanide in smoke by using terahertz waves. We will continue our investigation and clarify the sensing system's potential, such as the detectable gas species, detectable minimum gas concentrations, and maximum distance to the target. We will also clarify the needs of emergency responders and develop a more practical remote gas detection system.

References

[1] N. Shimizu, H.–J. Song, Y. Kado, T. Furuta, A. Wakatsuki, and Y. Muramoto, "Gas Detection Using Terahertz Waves," NTT Technical Review, Vol. 7, No. 3, 2009.
https://www.ntt-review.jp/archive/ntttechnical.php?contents=ntr200903sf7.html

[2] N. Shimizu, T. Ikari, K. Kikuchi, K. Matsuyama, A. Wakatsuki, S. Kohjiro, and R. Fukasawa, "Remote Gas Sensing in Full-scale Fire with Sub-terahertz Waves," 2011 IEEE MTT-S International Microwave Symposium Digest, Baltimore, MD, USA, 2011.

[3] A. Wakatsuki, Y. Muramoto, and T. Ishibashi, "Development of Terahertz-wave Photomixer Module Using a Uni-traveling-carrier Photodiode," NTT Technical Review, Vol. 10, No. 2, 2012.

https://www.ntt-review.jp/archive/ntttechnical.php?contents=ntr201202fa5.html
[4] S. Kohjiro, K. Kikuchi, M. Maezawa, T. Furuta, A. Wakatsuki, H. Ito, N. Shimizu, T. Nagatsuma, and Y. Kado, "0.2–0.5 THz Single-band Heterodyne Receiver Based on a Photonic Local Oscillator and a Superconductor-insulator-superconductor Mixer," Appl. Phys. Lett., Vol. 93, No. 9, p. 093508, 2008.
[5] K. Aihara and T. Kukutsu, "NTT R&D of Systems and Devices for Safety," NTT Technical Review, Vol. 10, No. 2, 2012. https://www.ntt-review.jp/archive/ntttechnical.php?contents=ntr201202fa1.html
[6] N. Shimizu, K. Kikuchi, T. Ikari, K. Matsuyama, A. Wakatsuki, S. Kohjiro, and R. Fukasawa, "Absorption Spectra of Smoke Emitted from Heated Nylon Fabric Measured with a Continuous-Wave Sub-Terahertz Spectrometer," Appl. Phys. Exp., Vol. 4, No. 3, pp. 032401–032401-3, 2011.

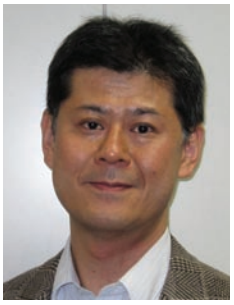

Naofumi Shimizu
Senior Research Engineer, Microwave and Photonics System Research Group, Smart Devices Laboratory, NTT Microsystem Integration Laboratories.
He received the B.E., M.E., and Ph.D. degrees in engineering physics from Kyoto University in 1986, 1988, and 2004, respectively. He joined NTT LSI Laboratories in 1988 and engaged in R&D of III-V high-speed devices. From 1998, he was with NTT Lightwave Communications Laboratory, where he was engaged in research on high-speed lightwave transport systems. In April 2004, he moved to NTT Microsystem Integration Laboratories and is currently engaged in R&D of terahertz spectroscopy systems. He is a member of IEEE, the Institute of Electronics, Information and Communication Engineers (IEICE), and the Japan Society of Applied Physics (JSAP). He received the 2002 IEICE Electronics Society Prize and the Best Paper Award of 2006 from the Asia-Pacific Microwave Photonics Conference.

Naoya Kukutsu
Senior Research Engineer, Supervisor, Group Leader, Smart Devices Laboratory, NTT Microsystem Integration Laboratories.
He received the B.E., M.E., and D.E. degrees in electrical engineering from Hokkaido University in 1986, 1988, and 1991, respectively. His D.E. dissertation described research for a time-domain electromagnetic wave numerical analysis method. In 1991, he joined NTT Applied Electronics Laboratories in Musashino. His current research involves millimeter-wave and terahertz-wave transmission, as well as imaging systems. He is a member of the IEEE MTT and COM Societies and IEICE.

Atsushi Wakatsuki
Senior Research Engineer, Terabit Device Laboratory, NTT Photonics Laboratories.
He received the B.E. and M.E. degrees in electronics from Tohoku University, Miyagi, in 1983 and 1985, respectively. He joined NTT in 1985 and developed telemetry and command equipment for communication systems on satellites. During 1989–1997, he moved to NTT Opto-Electronics Laboratories and ATR (Advanced Telecommunications Research Institute International) and studied semiconductor optical waveguide devices, MQW lasers, ultrashort-pulse generation, and two-light-mixing in nonlinear crystals. Since 2007, he has been with NTT Photonics Laboratories, where he has been active in research on ultrahigh-speed photodiodes and THz-wave photomixer modules. He is a member of the Japan Society of Applied Physics (JSAP).

Yoshifumi Muramoto
Senior Research Engineer, Terabit Device Laboratory, NTT Photonics Laboratories.
He received the B.E. and M.E. degrees in electrical engineering from Osaka Prefecture University in 1990 and 1992, respectively. He joined NTT Opto-Electronics Laboratories in 1992 and has been engaged in research on monolithically integrated photoreceivers and high-speed photodetectors. He is a member of IEICE and JSAP.

Development of Terahertz-wave Photomixer Module Using a Uni-traveling-carrier Photodiode

Atsushi Wakatsuki†, *Yoshifumi Muramoto, and Tadao Ishibashi*

Abstract

As a promising power source for various terahertz-wave (THz-wave) applications, we have developed a compact, lightweight, high-power, and ultrawideband THz-wave photomixer module using a uni-traveling-carrier photodiode. The module operates at room temperature and exhibits output power of over 0.5 mW at 0.35 THz and a 10-dB-down bandwidth of 260 GHz. Its output frequency can be swept continuously over an extremely wide frequency range in the terahertz band. In this article, we report on the photomixing technique using an ultrahigh-speed, high-power photodiode to generate THz-waves and the development of two versions of the photomixer module.

1. Introduction

In both communications and non-communications fields, there have been many trials for using an unexploited frequency range, the terahertz range, for high-frequency applications. Terahertz-waves (THz-waves) are electromagnetic waves in the frequency range from 0.1 THz to 10 THz (**Fig. 1**). This frequency range is positioned between radio waves and light waves, so the characteristics of THz-waves are either intermediate between them or a combination of their advantages. The main features of interest are also described in Fig. 1.

Recently, various high-frequency applications utilizing these superior features of THz-waves have been actively proposed and investigated. Possible applications include an ultrahigh-capacity wireless communication system, non-destructive inspection/imaging system, spectroscopic remote sensing/analysis system, and astronomical radio telescope system, as shown in **Fig. 2**. THz-waves have been enthusiastically investigated especially for systems concerning human safety and rescue in light of the frequent disasters that have occurred in recent years.

A compact, lightweight, and easy-to-handle THz-wave generator is a key device for such high-frequency systems. The development of a generator that simultaneously provides high power, a wide bandwidth, and frequency-sweeping capability has been one of the most important targets in this field.

2. THz-wave generation using a photodiode

NTT Photonics Laboratories invented the uni-traveling-carrier photodiode (UTC-PD) [1] as a key device for high-speed optical communication systems and has continued to investigate it to make improvements and develop applications. The UTC-PD simultaneously achieves both ultrahigh speed and high power compared with the conventional pin-PD. This excellent feature is extremely suitable not only for a high-speed optical communication receiver but also for an electromagnetic-wave generator. The development of the THz-wave photomixer module was based on the same technology as used in the UTC-PD-based millimeter-wave photomixer module that we developed earlier [2]. The structures of both

† NTT Photonics Laboratories
Atsugi-shi, 243-0198 Japan

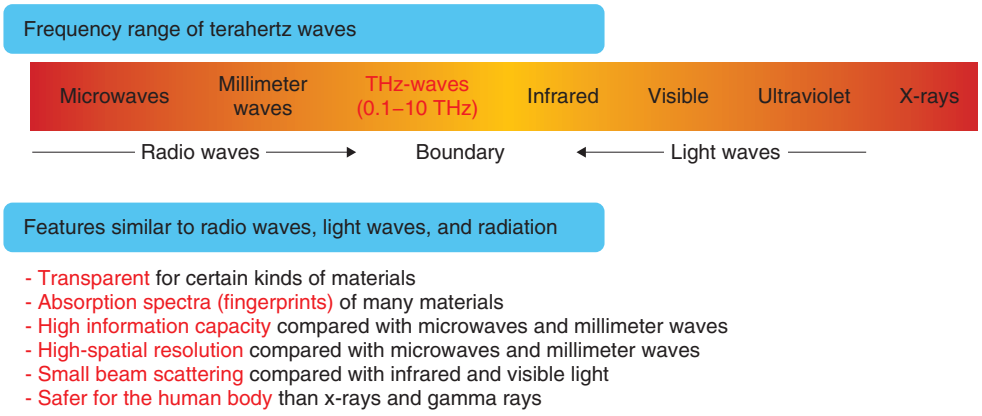

Fig. 1. Frequency range and interesting features of THz-waves.

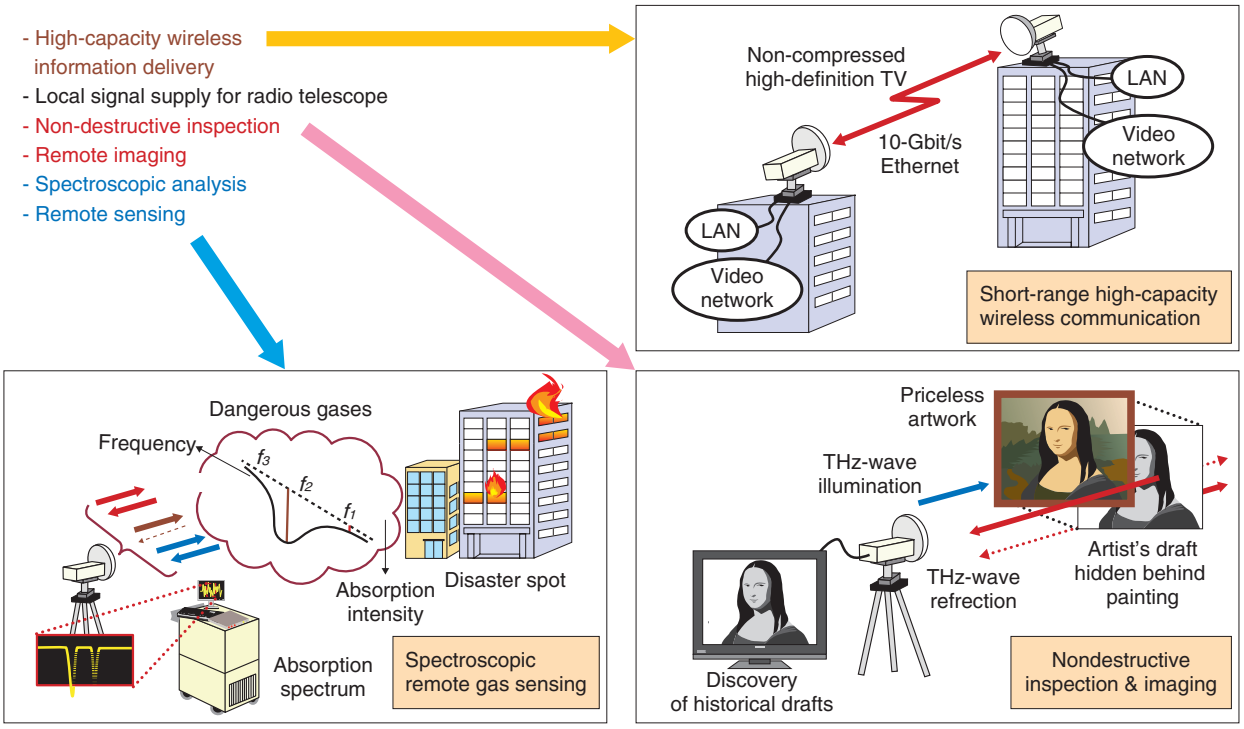

LAN: local area network

Fig. 2. Possible applications utilizing the features of THz-waves.

the UTC-PD and the module were improved and optimized for use in a frequency range of 0.2 THz to 0.65 THz. At present, our module has a center frequency of 0.35 THz for application as the power source of a spectroscopic remote sensing system [3].

The PD-based photomixing technique is explained in **Fig. 3**. THz-waves are generated by ultrahigh-speed optical-to-electrical (O/E) conversion in a UTC-PD. An optical beat-signal with a beating frequency of f_b (= f_1 - f_2) is obtained by combining two lights of different frequencies (f_1, f_2; f_1>f_2) in an optical coupler. For example, by using lights with

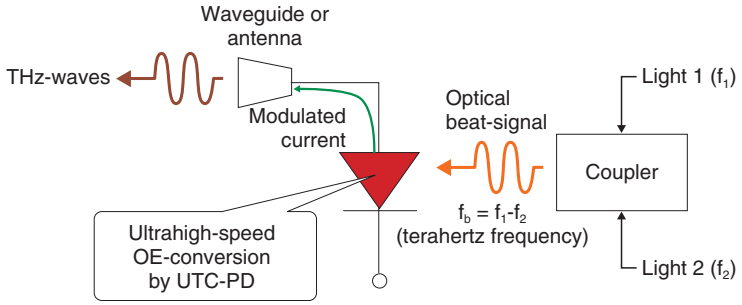

Fig. 3. PD-based photomixing technique.

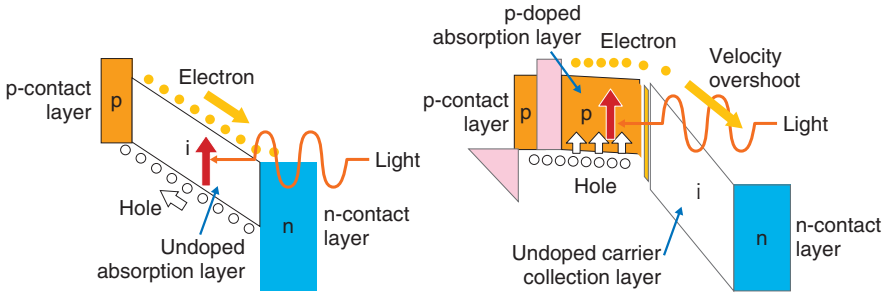

(a) Band structure of pin-PD (b) Band structure of UTC-PD

Fig. 4. Differences between band structures of conventional pin-PD and UTC-PD.

wavelengths of 1.5000 μm (201 THz) and 1.5075 μm (200 THz), we can get a beat signal with a frequency of exactly 1 THz. The optical beat-signal that is input into the UTC-PD is converted into a modulated electric current with the same frequency as f_b. THz-waves can be obtained by radiating the modulated current into space from a waveguide or antenna.

Details of the UTC-PD used in the photomixing technique are given in the next section.

3. UTC-PD

3.1 Features

Although the most widely used PD is the conventional pin-PD, there are two limitations regarding its performance (pin: positive, intrinsic, negative layers). One concerns the maximum operating speed. When lights are input into the pin-PD's absorption layer, electron-hole pairs, which are the electric current carriers, are generated (**Fig. 4(a)**). In a pin-PD, both electrons and holes contribute to its O/E-conversion mechanism. Because a hole's effective mass is larger than an electron's and its velocity is much lower, the maximum operating speed of the pin-PD is limited by the hole velocity. The other limitation concerns the maximum output current. When the optical input power becomes higher, the band in the undoped absorption layer is bent by the space charge due to carrier accumulation. This band bending causes a drastic reduction in carrier velocity, which results in saturation of the output current. To overcome these limitations of the pin-PD, we studied the UTC-PD.

In the UTC-PD, a p-doped absorption layer is separated from a wide-gap undoped carrier collection layer (**Fig. 4(b)**), which is in clear contrast to the pin-PD. This structure means that only electrons are the active carriers running through the depleted undoped carrier collection layer. Most of the photogenerated holes relax extremely quickly into the absorption layer where holes are the major carrier. Consequently, the maximum operating speed of the UTC-PD is determined only by the electron velocity, which is much higher than the hole velocity. The space charge effect is also much smaller than in the pin-PD because

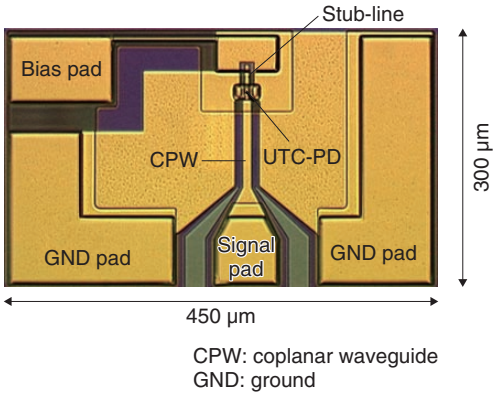

Fig. 5. Photograph of the fabricated UTC-PD chip.

carrier accumulation is extremely small in principle compared with the pin-PD. For these reasons, the UTC-PD can exhibit high performance, that is, ultra-high-speed and high saturation output current simultaneously.

We have achieved a 3-dB-down bandwidth of 310 GHz and a 10-dB-down bandwidth of 750 GHz as the operational frequency bandwidth [4]. We have also obtained a maximum output current of 30 mA for high optical input power.

3.2 Optimization for THz-wave photomixer module

It is essential to optimize the UTC-PD's band structure in order to obtain an output current with a terahertz frequency. We designed a thinner absorption layer than the one in the UTC-PD for the previous millimeter-wave photomixer; this reduced the UTC-PD's carrier transit time when it operates at higher frequencies. The thicknesses and materials of the other layers were also optimized for compatibility with the thin absorption layer.

Besides the band structure, we also improved the physical structure of the UTC-PC chip. The fabricated UTC-PD chip designed to operate in the terahertz frequency range is shown in **Fig. 5**. The chip is 300 × 450 µm^2.

The frequency response of the PD output current shows a generally broadband-shape caused by the resistor-capacitor time constant. The response decreases with increasing operating frequency. For the THz-wave photomixer, a stub-line was integrated on the chip to increase the output current. It acts as a resonant circuit for the UTC-PD to compensate for the roll-off of the frequency response. The output power of the THz-waves is designed to be as high as possible at around the designed center frequency. In this development, the center frequency was set to 0.35 THz. The output current is expected to increase at around the center frequency through use of the resonant effect. We measured the pulse photoresponse to evaluate the chip's resonant design. From the measured pulse waveform oscillating at about 0.35 THz, we ascertained that the stub-line acted properly as a resonant circuit.

4. Waveguide-output-type photomixer module

4.1 Optimization

For practical use, in addition to being high-performance, the photomixer module is required to be compact, lightweight, and easy to handle. Moreover, since the module will be applied to various high-frequency systems, it should be easy to assemble on a board or in a package. As a result of our investigation, we determined that a butterfly-package would be an excellent form for the module. It is a generic package with a good track record for many optical devices, so it is cheap and readily available.

For the module structure investigation, there are two main issues: they concern optical implementation and electrical implementation. The former covers how efficiently light is input to the UTC-PD, and the latter covers how efficiently ultrahigh-frequency current from the UTC-PD is converted into THz-waves.

Today's high-frequency coaxial connectors have pronounced propagation loss for current with a frequency range above 0.1 THz, so it is essential to chose either the waveguide technique or direct

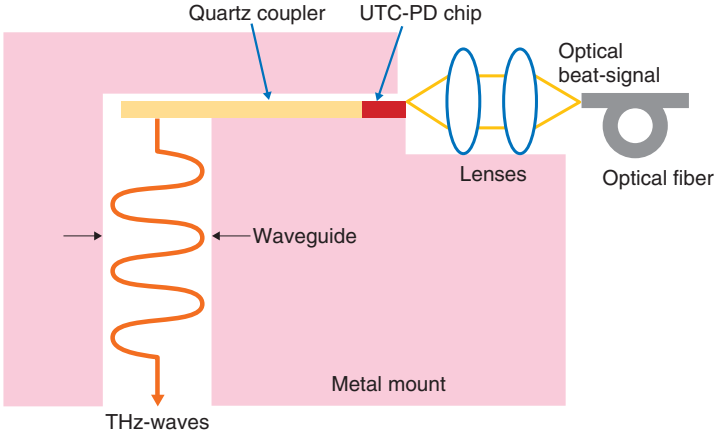

Fig. 6. Schematic cross-section of the module's internal structure.

radiation technique (quasi-optical technique) to output the current from the module. We developed a waveguide-based module structure during our development of the previous millimeter-wave photomixer module and confirmed its excellent characteristics. The THz-wave photomixer module is based on an extension of that technique.

The cross-section of the internal structure is schematically shown in **Fig. 6**. The optical part consists of an optical fiber and collimation lenses. The collimation lens system has good versatility for an optical design, and it also has excellent optical alignment stability among the optical fiber, lenses, and UTC-PD. The UTC-PD chip is mounted on a metal block with a rectangular waveguide whose aperture size is 0.864 mm × 0.432 mm. The UTC-PD chip and the waveguide are connected by a quartz coupler consisting of an impedance converter, a micro-strip line, and a radiator. The module is made by assembling these components in the butterfly-package with the same waveguide.

The design of the quartz coupler is extremely important for high emission efficiency of the ultra-high-frequency current as THz-waves into the waveguide. The design policies were as follows:

(1) Reflection power as low as possible
(2) Transmission power as high as possible
(3) Propagation of higher-order modes in the waveguide suppressed as much as possible from the UTC-PD's current output point to the waveguide's THz-wave output point.

The quartz coupler was designed using a three-dimensional electromagnetic wave simulator to obtain flattened characteristics from 0.2 THz to 0.65 THz. As a result of simulation for various designs, the optimized one achieved reflection power of less than -30 dB and transmission power loss of less than 3 dB.

4.2 Performance

We fabricated a THz-wave photomixer module (**Fig. 7**) with the optimized design described in the previous section. The module is 3 × 1.65 × 1 cm^3.

The output power dependence on frequency when the optical beat signal's frequency was swept from 0.2 THz to 0.65 THz is shown in **Fig. 8**. The output power was clearly enhanced at around 0.35 THz (designed center frequency of the stub-line) with the maximum value being over 0.5 mW [5]. This is the highest value ever reported for a photomixer with a single PD operating in this frequency range. The 3- and 10-dB-down bandwidths were as wide as 120 and 260 GHz, respectively, showing extremely wideband performance.

The main feature of this module is that it simultaneously achieves both high-output power and extremely wide bandwidth. In addition to this high performance, it is very easy to use because it operates in continuous-wave operation at room temperature without any cooling.

5. Quasi-optical photomixer module

For diversification of the THz-wave output method, we have been also investigating a quasi-optical photomixer module (**Fig. 9**). The THz-wave generation principle is the same as for the waveguide-output-type module. The quasi-optical module consists of a

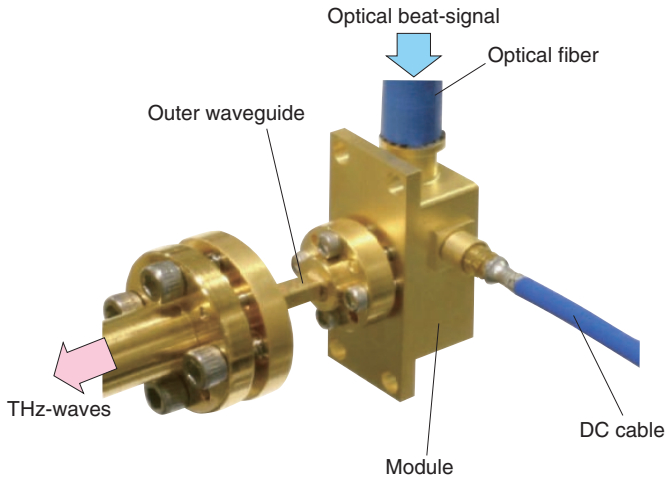

Fig. 7. Photograph of the fabricated THz-wave photomixer module.

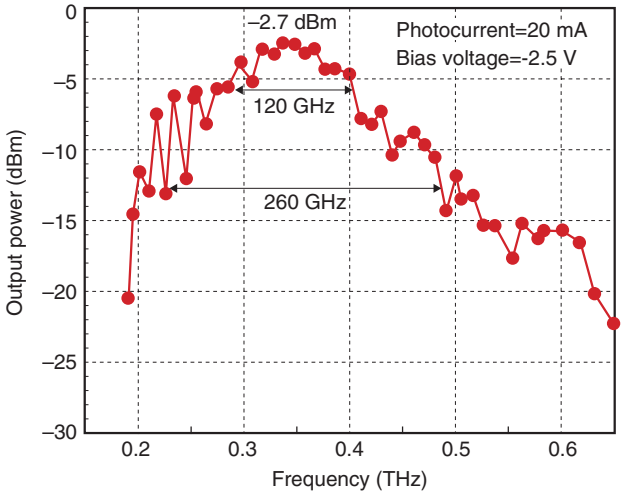

Fig. 8. Fabricated module's output power dependence on frequency.

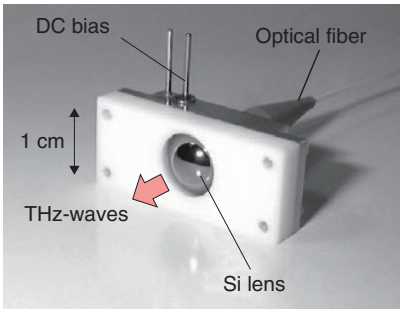

Fig. 9. Photograph of the quasi-optical photomixer module.

UTC-PD chip integrated with an antenna and a metal package with a silicon lens for collimating the radiated THz-waves.

In the waveguide-output-type module, as the operation frequency becomes higher, the waveguide's aperture must become smaller. Therefore, in the terahertz range, it becomes difficult to fabricate a precise rectangular waveguide with a small aperture by a metal-cutting process. The quasi-optical module is suitable for increasing the operating frequency because it does not require high-precision metal-cutting. There are also some other good features:

(1) It is easy to make either a broadband- or resonant-type module by choosing the type of integrated antenna.
(2) It is easy to fabricate an airtight module, which is beneficial for module reliability because the module does not have an aperture.
(3) The electrical implementation is easy because that there is no quartz coupler requiring precise positional alignment.

Although the maximum output power is lower than that of the waveguide-output-type module at present, we confirmed THz-wave generation up to a frequency of 1.5 THz [6].

5. Conclusion

The features of the UTC-PD were described, including the operating principles and characteristics.

Compared with the conventional pin-PD, the UTC-PD has the advantages of extremely wide bandwidth and high power owing to its unique carrier transport mechanism. One application for the UTC-PD is THz-wave generation. Our developed THz-wave photomixer module using a UTC-PD, fabricated as a waveguide-output-type module, exhibits excellent performance. It has a maximum output power of over 0.5 mW at 0.35 THz and a 10-dB-down bandwidth of 260 GHz. This maximum output power is the highest value ever reported for direct generation from a photomixer operating in a frequency range of 0.2 THz to 0.65 THz. Our UTC-PD-based quasi-optical module generates THz-waves up to a maximum frequency of 1.5 THz.

Acknowledgment

Part of this work was supported by the National Institute of Information and Communications Technology, Japan.

References

[1] T. Ishibashi and H. Ito, "Uni-traveling-carrier Photodiodes," Tech. Dig. Ultrafast Electronics and Optoelectronics, Lake Tahoe, CA, USA, pp. 83–87, 1997.
[2] H. Ito, T. Nagatsuma, A. Hirata, A. Sasaki, Y. Hirota, and T. Ishibashi, "High-power Photonic Millimeter-wave Generation at 100 GHz Using Matching-circuit-integrated Uni-travelling-carrier Photodiodes," Proc. of Inst. Elect. Eng. Optoelectron., Vol. 150, pp. 138–142, 2003.
[3] N. Shimizu, N. Kukutsu, A. Wakatsuki, and Y. Muramoto, "Remote Detection of Hazardous Gases in Full-scale Simulated Fire by Using Terahertz Electromagnetic Waves," NTT Technical Review, Vol. 10, No. 2, 2012.
https://www.ntt-review.jp/archive/ntttechnical.php?contents=ntr201202fa4.html
[4] H. Ito, T. Furuta, S. Kodama, and T. Ishibashi, "InP/InGaAs Uni-traveling-carrier Photodiode with 310 GHz Bandwidth," Electron. Lett., Vol. 36, No. 21, pp. 1809–1810, 2000.
[5] A. Wakatsuki, T. Furuta, Y. Muramoto, T. Yoshimatsu, and H. Ito, "High-power and Broadband Sub-terahertz Wave Generation Using a J-band Photomixer Module with Rectangular-waveguide Output Port," Proc. of the 33rd IRMMW-THz2008, Pasadena, CA, USA, M4K2.1199, 2008.
[6] H. Ito, T. Furuta, F. Nakajima, K. Yoshino, and T. Ishibashi, "Photonic Generation of Continuous THz Wave Using Uni-traveling-carrier Photodiode," J. Lightwave Technol., Vol. 23, No. 12, pp. 4016–4021, 2005.

Atsushi Wakatsuki
Senior Research Engineer, Terabit Device Laboratory, NTT Photonics Laboratories.
He received the B.E. and M.E. degrees in electronics from Tohoku University, Miyagi, in 1983 and 1985, respectively. He joined NTT in 1985 and developed telemetry and command equipment for communication systems on satellites. During 1989–1997, he moved to NTT Opto-Electronics Laboratories and ATR (Advanced Telecommunications Research Institute International) and studied semiconductor optical waveguide devices, MQW lasers, ultrashort-pulse generation, and two-light-mixing in nonlinear crystals. Since 2007, he has been with NTT Photonics Laboratories, where he has been active in research on ultrahigh-speed photodiodes and THz-wave photomixer modules. He is a member of the Japan Society of Applied Physics (JSAP).

Yoshifumi Muramoto
Senior Research Engineer, Terabit Device Laboratory, NTT Photonics Laboratories.
He received the B.E. and M.E. degrees in electrical engineering from Osaka Prefecture University in 1990 and 1992, respectively. He joined NTT Opto-Electronics Laboratories in 1992 and has been engaged in research on monolithically integrated photoreceivers and high-speed photodetectors. He is a member of the Institute of Electronics, Information and Communication Engineers (IEICE) and JSAP.

Tadao Ishibashi
Research Professor at NTT Photonics Laboratories and Engineering Manager at NTT Electronics Corporation.
He received the B.E., M.E., and Ph.D. degrees in applied physics from Hokkaido University in 1971, 1973, and 1986, respectively. Since joining Nippon Telegraph and Telephone Public Corporation (now NTT) in 1973, he has been involved in research on high-speed and optoelectronic semiconductor devices, including IMPATT diodes, field-effect transistors, heterostructure bipolar transistors, high-speed photodiodes, avalanche photodiodes, THz photomixers, and Mach-Zehnder modulators. He received the Ichimura Award in 1992 and IEICE Electronics Society Award in 2001. He is a fellow of IEICE, JSAP, and IEEE.

Visualization of Pharmaceutical Drug Molecules by Terahertz Chemical Imaging

Katsuhiro Ajito[†], *Yuko Ueno, and Ho-Jin Song*

Abstract

Terahertz spectroscopy allows the detection and identification of various molecular networks of chemical bond interactions, including those of hydrogen bonds. In this article, we explain terahertz time-domain spectroscopy, the principles of terahertz chemical imaging, and a multicomponent quantitative analysis method for amino acids that can visualize pharmaceutical crystalline polymorphs as an example of this technology.

1. Introduction

Terahertz waves (THz-waves), which possess an energy level between that of radio waves and light waves, can provide various types of information, including crystal phonon modes, low-wavenumber frequencies, and gas molecule rotation modes. The specific absorption frequencies of a chemical substance are shown in **Fig. 1** [1]. Mid-wavelength infrared absorption spectroscopy deals with the high-frequency vibration mode, so it can identify the functional groups of molecules. By contrast, terahertz spectroscopy can determine low-frequency vibration modes such as those existing in van der Waals interactions and hydrogen bonding. Terahertz peaks appear owing to resonance in the hydrogen bonds in most amino acid crystals. Terahertz spectroscopy can identify various types of information from molecular networks, including biomolecules dissolved in aqueous solution, organic molecular crystals, higher-order protein structures, and the DNA (deoxyribonucleic acid) double helix. The hydrogen bonding of biomolecule clusters and molecular networks in water is shown in **Fig. 2**. From the terahertz spectrum, we can obtain the continuous frequency corresponding to each individual peak; that is, we can obtain the chemical image. Molecular clusters may contain pharmaceutical drug molecules and hydrogen molecules, amongst others. These molecular networks are important in the biomedical field because they can influence the effectiveness of medicines. However, the details of molecular networks are difficult to obtain because the cluster size is on the nanometer scale and there are few methods for measuring such sizes accurately, particularly when the cluster includes water as a component.

The resonance frequency of molecular networks is in the terahertz band, which makes such networks amenable to terahertz spectroscopy and imaging. Terahertz spectroscopy is a useful tool that can identify hydrogen bonds present in molecules that comprise various bio-specimens, including organic acids, amino acids, sugars, drugs, polypeptides, DNA, and proteins as well as macrostructures such as cancer cells. Since most amino acids and pharmaceutical drug molecules contain hydrogen bonds, quantitative analysis from terahertz spectrum peaks is possible. The applications of terahertz spectroscopy are wide ranging and many practical uses are expected. In addition to fundamental research applications such as pathology testing or the identification of different types of explosives, other applications of the technology have been receiving attention. In contrast to X-ray imaging, terahertz chemical imaging (TCI) can identify molecules by their molecular network

† NTT Microsystem Integration Laboratories
Atsugi, 243-0198 Japan

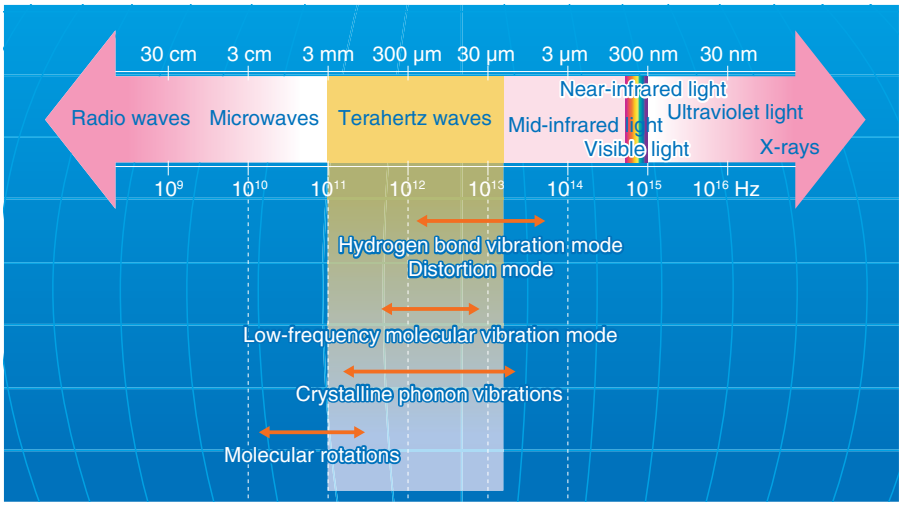

Fig. 1. Specific chemical absorption frequencies.

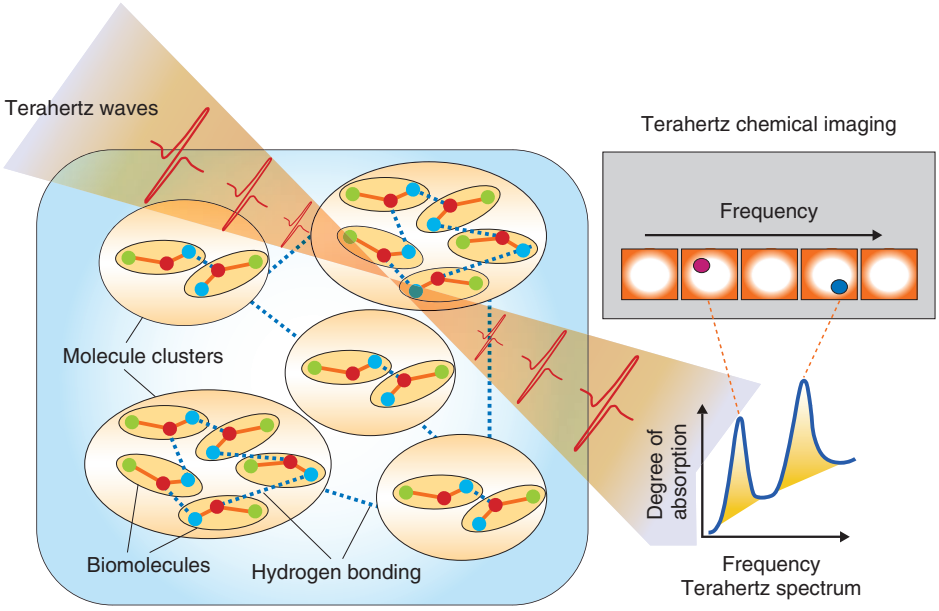

Fig. 2. Terahertz spectrum of molecular network.

spectrum. Because the technique can reveal the molecular network rather than only the molecular distribution, we believe that TCI can provide a new method for both drug identification and pathological examination. Terahertz waves penetrate many types of materials and can be used to confirm molecular uniformity as well as to identify crystal polymorphs. Crystal polymorphism arises from different types of hydrogen bonding occurring within crystals and can lead to differences in physical and chemical properties, including differences in solubility, melting point, and bioavailability. Bioavailability, rather than describing physiochemical properties of pharmaceutical drug molecules, describes the way in which chemicals are absorbed in the human body and is important in determining the effective dosages of particular medications.

2. Principle of terahertz time-domain spectroscopy (THz-TDS) and THz-TDS system

Terahertz time-domain spectroscopy (THz-TDS) is the most popular type of terahertz spectroscopy. Advances in terahertz technology have allowed the commercialization of THz-TDS, which is also beginning to be recognized as a new analytical chemistry method. A THz-TDS system involves coherent signal generation and detection. The terahertz pulse repetition frequency is around 80 MHz. A typical THz-TDS system configuration is shown in **Fig. 3** [2]. An ultrashort (10–100 fs) laser pulse is split so that both the terahertz generator and receiver are irradiated. The most common terahertz generator and receiver is a photoconducting antenna. A sub-picosecond terahertz pulse wave irradiates the sample and when it propagates, the electric field strength changes. Rather than measuring the light intensity in the frequency domain, we use the time domain to measure the electric field strength. The measurement of terahertz waves in the frequency domain usually uses a delay line. Repetitive terahertz pulse waves are measured and converted into intensity and phase by Fourier transformation. THz-TDS can be performed at room temperature and it has better sensitivity than far-infrared spectroscopy for frequency domain measurement. An example of a TCI system using THz-TDS and a stage that can be moved in three dimensions is shown in **Fig. 4** [3]. While the stage is scanned, the waveform of the terahertz pulse wave is measured and recorded and then the Fourier transform is used to change each frequency. Samples such as medicinal tablets are fixed in a vacuum chamber, which can attenuate the absorption of atmospheric water.

3. Quantitative chemical analysis by THz-TDS

Until now, there has been no discussion of the quantitative relationship between the degree of absorption (absorbance) gained from THz-TDS and the sample concentration or sample optical path length measured from actual spectra. To illustrate the usefulness of THz-TDS as a general analytical sensing method, it is

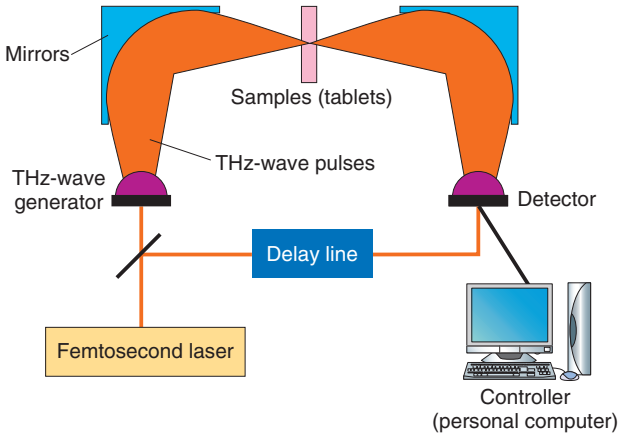

Fig. 3. THz-TDS system configuration.

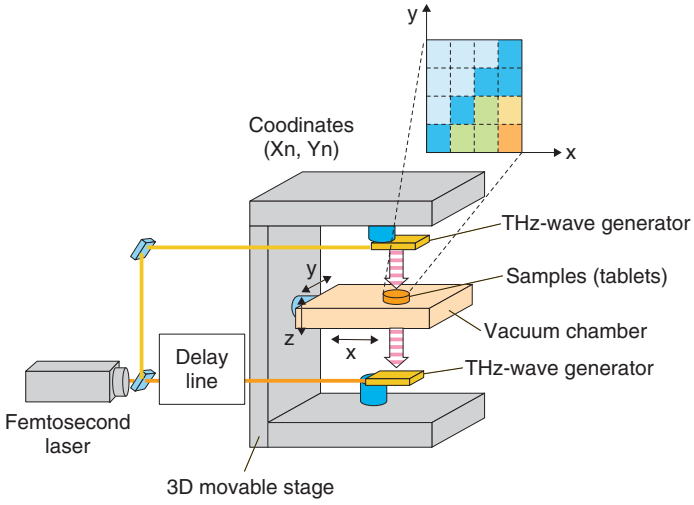

Fig. 4. TCI system using a three-dimensionally movable stage.

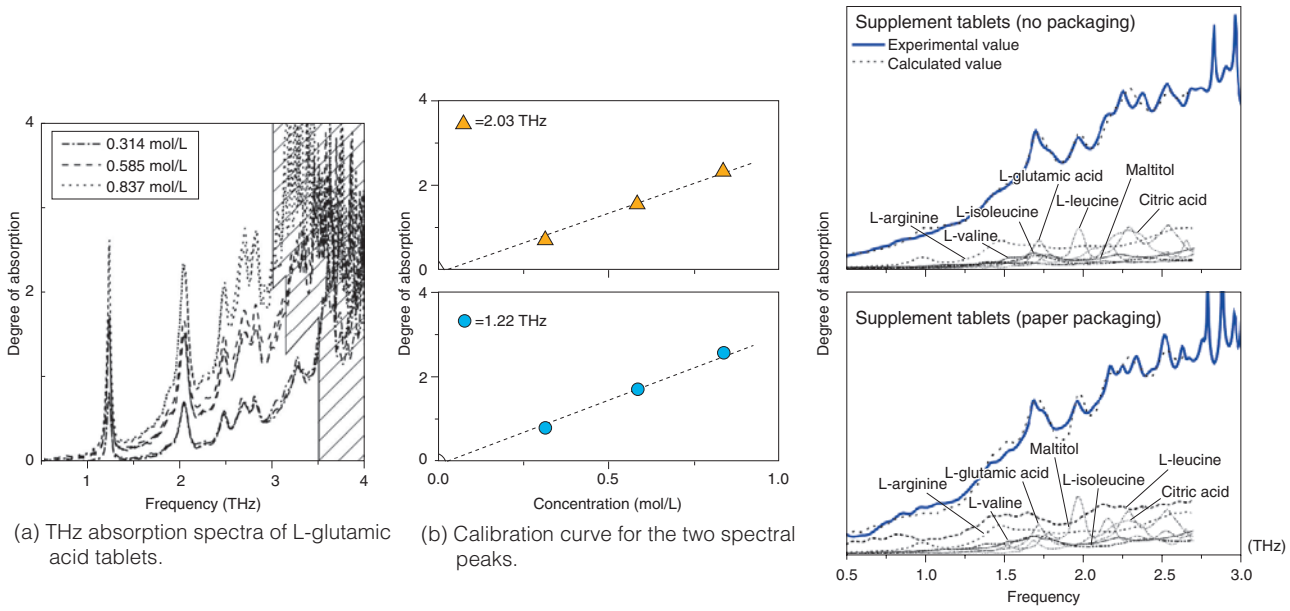

(a) THz absorption spectra of L-glutamic acid tablets.

(b) Calibration curve for the two spectral peaks.

(c) Spectra of supplement tablets and results of quantification analysis based on standard spectra.

Fig. 5. THz quantification analysis results for supplement tablets containing various types of amino acids.

necessary to conduct a quantitative discussion of the relationship between absorbance and sample concentration or sample optical path length and the relationship between noise level and detection limit, in parallel with qualitative discussion of the terahertz absorption peaks. The absorption spectra of three different concentrations of medicinal tablets that include crystals of the essential amino acid L-glutamic acid are shown in **Fig. 5(a)** [4]. Amino acid crystals form a stable crystal structure via hydrogen bonding among amino acid molecules or bonding between amino acid molecules and hydrated water molecules. It is believed that multiple instances of hydrogen bonding exist between molecules, which can be reflected in a single spectrum. The calibration curves for the two main peaks are shown in **Fig. 5(b)**. The peak intensity (including background absorption) is proportional to the concentration, which shows that quantitative analysis is possible. To determine the types of different amino acids present, we calculated the molar absorption coefficients in the region from 0.5–3.0 THz. These coefficients were then used as the standard spectra. We then carried out quantitative chemical analysis of sample tablets containing a mixture of several amino acids. The upper part of **Fig. 5(c)** shows the spectrum of commercially available supplements containing various types of amino acids [5]. Five types of amino acid were detected, including L-glutamic acid, and L-leucine, and the concentration of each amino acid could be quantified by automatic analysis using a standard spectrum database. The lower part of Fig. 5(c) shows the spectrum and analysis result for pills wrapped in medical paper made from starch. Since THz-waves have high permeability for such substances even when they are wrapped in medical paper, there was almost no resulting effect on peak position and strength, and quantitative analysis was possible with standard spectra. We expect the quantitative accuracy to improve in the future as the database quality and the fitting techniques are improved.

4. Visualization of pharmaceutical drug molecules by TCI

TCI technology can identify the two- or three-dimensional distribution of each type of molecule on the basis of the molecular network as well as molecular concentrations from the terahertz absorption spectrum. An example of an application to pharmaceutical drug molecules—identification of two polymorphs of famotidine, which is a component of stomach medicine and a histamine receptor antagonist (H2 blocker)—is shown in **Fig. 6**.

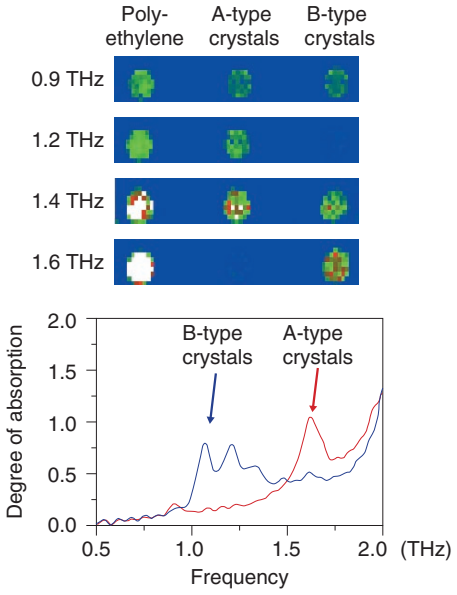

(a) Terahertz absorption spectra and transmittance images of a tablet of crystalline polymorphic famotidine.

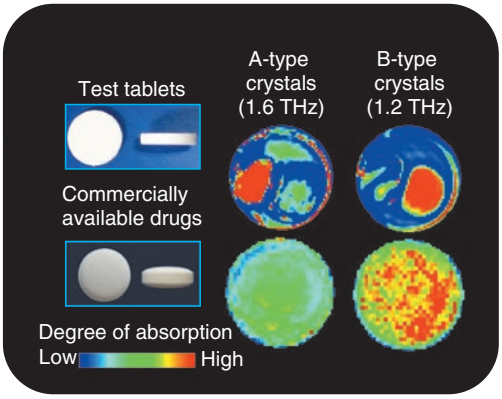

(b) Terahertz absorbance images of test and commercial tablets.

Fig. 6. TCI mapping of test and commercial drug tablets.

The absorption spectra of tablets containing the A-type and B-type crystalline polymorphs of famotidine with polyethylene binder as well as transmittance TCI images are shown in Fig. 6(a) [6]. Type B is a digestive-tract medicine that works as a histamine H2-receptor antagonist. Types A and B are easily identified in the terahertz spectrum because there are differences in their absorption peaks. Absorption images of the test tablets, which exhibited the characteristic A-type and B-type peaks, and of commercial drug tablets are shown in Fig. 6(b) [7]. The A-type and B-type tablets were 10 mm and 7.6 mm, respectively, in diameter. Types A and B showed peaks close to 1.6 THz and 1.2 THz, respectively. In the test tablets, regions of A type on the left and regions of B type on the right could be clearly identified. By contrast, in the commercial drug tablet images, there is almost no A type, whereas B type is widely distributed as the active ingredient. This is the first time that pharmaceutical drug crystal polymorphs have been visualized inside tablets. There are several tablet molding methods, so the method used for molding the test tablets investigated here may not be used for all tablets in practice; nevertheless, it is very important to pioneer new testing methods while achieving the desired goal of pharmaceutical product safety.

5. Conclusion

We introduced molecular pharmaceutical drugs and supplements as examples of substances suitable for quantitative analysis by terahertz spectroscopy and chemical imaging. Even though the number of researchers involved in terahertz wave technology has increased markedly in recent years, potential applications of terahertz wave chemical analysis are only just being identified. The reasons for this include, but are not limited to, the difficulty in measuring the 1–3-THz range, which is effective for detecting hydrogen bonding and molecular networks, the fact that a theory for terahertz spectral analysis methods has not yet been established, the complexity of THz-TDS spectral analysis, and the cost of the equipment used. Nevertheless, the ability of terahertz waves to visualize new structures and interactions that were previously unobservable is a powerful tool in the fields of biology, medicine, and life sciences. In future, we would like to continue exploring and developing this revolutionary technology.

References

[1] Y. Ueno and K. Ajito, "Analytical Terahertz Spectroscopy," Analytical Sciences, Vol. 24, No. 2 pp. 185–192, 2008.

[2] K. Ajito, Y. Ueno, T. Haga, and N. Kukutsu, "Terahertz Spectroscopy Technology for Molecular Networks," NTT Technical Review, Vol. 7, No. 3, 2009.
https://www.ntt-review.jp/archive/ntttechnical.php?contents=ntr200903sf6.html

[3] Y. Ueno, R. Rungsawang, I. Tomita, and K. Ajito, "Quantitative Measurements of Amino Acids by Terahertz Time-domain Transmission Spectroscopy," Analytical Chemistry, Vol. 78, No. 15, pp. 5424–5428, 2006.

[4] Y. Ueno, K. Ajito, N. Kukutsu, and E. Tamechika, "Quantitative Analysis of Amino Acids in Dietary Supplements Using Terahertz Time-domain Spectroscopy," Analytical Sciences, Vol. 27, No. 4, pp. 351–356, 2011.

[5] K. Ajito, Y. Ueno, H.-J. Song, E. Tamechika, and N. Kukutsu, "Terahertz Chemical Imaging of Molecular Networks for Pharmaceutical Applications," ECS Trans., Vol. 35, No. 7, pp. 157–165, 2011.

[6] K. Ajito and Y. Ueno, "THz Chemical Imaging for Biological Applications," IEEE Trans. on Terahertz Science and Technology, Vol. 1, No. 1, pp. 293–300, 2011.

[7] K. Ajito, Y. Ueno, H.-J. Song, E. Tamechika, and N. Kukutsu, "Terahertz Spectroscopic Imaging of Polymorphic Forms in Pharmaceutical Crystals," Molecular Crystals and Liquid Crystals, Vol. 538, No. 1, pp. 33–38, 2011.

Katsuhiro Ajito

Senior Research Scientist, Smart Devices Laboratory, NTT Microsystem Integration Laboratories, and Distinguished Technical Member, NTT Science and Core Technology Laboratory Group.

He received the Ph.D. degree in applied chemistry from the University of Tokyo in 1995. He joined NTT Basic Research Laboratories in 1995. From 1995 to 2007, he studied glutamate in single synapses using Raman spectroscopy and laser tweezers. His current research interests include nano- and biochemistry studied by terahertz spectroscopy and imaging techniques. He received the Young Scientist Award for the Presentation of an Excellent Paper from the Japan Society of Applied Physics (JSAP) in 1999. He has been the Executive Director and the Chair of the Terahertz Spectroscopy Division of the Spectroscopical Society of Japan (SSJ) since 2005, the Secretary of the Terahertz Interest Group in IEEE 802.15 Working Group for wireless personal area networks since 2011, and the Chair of the Micro/Nano Electromechanical Systems and Bio/Medical Analyses Area of the International Conference on Solid State Devices and Materials in JSAP since 2012. He is a member of IEEE, SSJ, JSAP, the Chemical Society of Japan, and the American Chemical Society.

Yuko Ueno

Senior Research Scientist, Network Hardware Integration Laboratory, NTT Microsystem Integration Laboratories.

She received the B.S., M.S., and Ph.D. degrees in chemistry from the University of Tokyo in 1995, 1997, and 2002, respectively. She joined NTT Integrated Information & Energy Systems Laboratories in 1997. She was a post-doctoral fellow at the University of California at Berkeley and at Lawrence Berkeley National Laboratory, Berkeley, CA, USA, from 2004 to 2005. She received the Encouragement Award (award for a young scientist) from the Japan Society for Analytical Chemistry.

Ho-Jin Song

Research Engineer, NTT Microsystem Integration Laboratories.

He received the B.S. degree in electronics engineering from Kyungpook National University, Korea, in 1999 and the M.S. and Ph.D. degrees in information and communications engineering from Gwangju Institute of Science and Technology (GIST), Korea, in 2001 and 2005, respectively. From 2005 to 2006, he was at the Center for Hybrid Optical Access Networks (CHOAN) in GIST, Korea, as a research professor and engaged in research on millimeter-wave communications systems utilizing radio-over-fiber technologies. Since joining NTT Microsystem Integration Laboratories in 2006, he has been working on the development of millimeter-wave and sub-terahertz wave systems for communications, sensing, imaging, and measurement applications using photonic technologies and high-speed electronics. He is a member of IEEE and IEICE.

Portable Sensor for Determining Benzene Concentration from Airborne/liquid Samples with High Accuracy

Serge Camou[†], *Emi Tamechika, and Tsutomu Horiuchi*

Abstract

Our previously developed portable monitoring system for detecting airborne benzene down to the level of one part per billion (1 ppb) has been extended to a portable sensor for liquid samples through the development of modules for extraction from the liquid phase to the vapor phase based on two protocols: bubbling and pervaporation. This portable sensor has demonstrated a high selectivity to benzene or a detection limit below the one-part-per-billion-by-volume (1-ppbV) level depending on the extraction protocol.

1. Introduction

Benzene, toluene, and xylenes, sometimes referred to as BTX, have similar chemical compositions but exhibit specific properties that have led to their extensive usage in various industries (chemical industries and petroleum refineries) and in commonly used products (e.g., gasoline). However, all three compounds, but especially benzene, represent threats to human health even at trace-level concentrations. On the basis of scientific studies, developed countries have set regulatory levels that should not be exceeded in gas and liquid samples in order to prevent any impact on the human population or environmental ecosystems. Regulatory levels in Japan, the USA, and Europe are given in **Table 1**. Because of its large carcinogenic effect, benzene has the lowest regulatory levels, in the low-parts-per-billion (ppb, 10^{-9}) range. Standard protocols for detecting BTX compounds have been developed, mostly on the basis of the gas chromatography and mass spectrometry (GC/MS) technique. This setup provides high reliability and sensitivity; however, it cannot be operated in the field, requires a highly skilled operator, and is costly and bulky.

† NTT Microsystem Integration Laboratories
Atsugi-shi, 243-0198 Japan

Between the two main potential exposure media, liquid and gas, airborne BTX is considered to be the major threat because car exhaust has been identified as the main source of emission. This is particularly relevant in densely populated areas with huge numbers of cars on the roads.

For simultaneous detection of BTX compounds on-site with a portable sensor, absorption spectroscopy in the ultraviolet (UV) optical wavelength range represents a promising alternative. In the UV wavelength range, almost all of the molecules absorb light at various wavelengths depending on the structure of their outer electron clouds. For simultaneous detection of multiple compounds, the wavelength range can be tuned to where compounds of interest exhibit strong and characteristic absorption peaks. For example, benzene, toluene, and o-xylene exhibit very distinct and well-resolved absorption signatures in the 230–290-nm range (**Fig. 1**) despite their similar chemical compositions. When operating in this wavelength range, this technique therefore enables simultaneous detection of the three compounds. However, the sensitivity is usually limited by the length of the light path through the sample, with the typical detection limit being in the parts-per-million (ppm, 10^{-6}) range. To reach sensitivity in the parts-per-trillion (ppt, 10^{-12}) range and satisfy the requirements, one usually uses a pre-concentration cell before the

Table 1. Datasheet for benzene, toluene, and xylene (o-, p-, and m-xylene all together) for Japan, the USA, and Europe.

	Boiling point (°C)	Solubility in water (g/L)	Air (ppb)			Waste water (ppbV)			Drinking water (ppbV)		
			Japan	USA*	Europe	Japan	USA	Europe	Japan	USA	Europe
Benzene	80.5	1.8	1	10^3	1.7	110	500	–	11	5	1
Toluene	110.8	0.47	70	$2x10^5$	–	–	–	–	–	1000	–
Xylene	138–144	ca. 0	200	10^5	–	–	–	–	–	10,000	–

* In the workplace (8-hour workday or 40-hour workweek exposure)

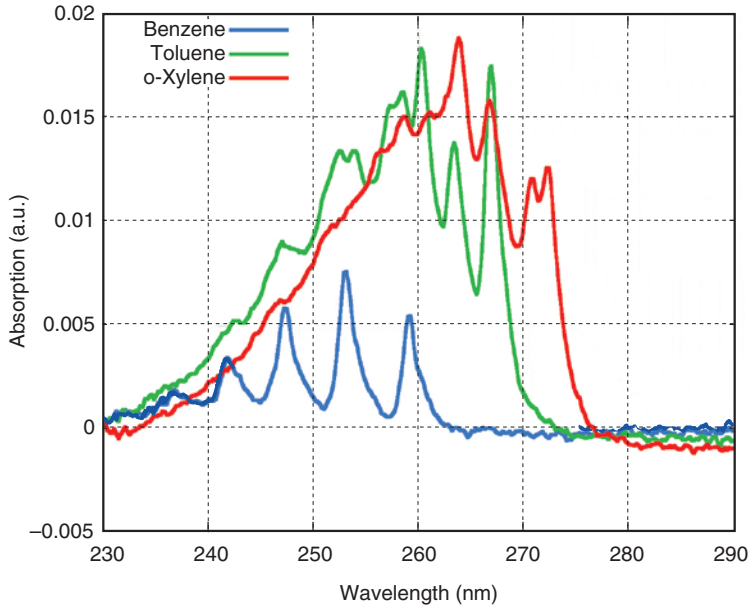

Fig. 1. Reference absorption spectra of benzene, toluene, and o-xylene in the 230–290-nm wavelength range.

detection cell. The sample gas is enriched by accumulating molecules from the carrier gas over a period of time (concentration time) and releasing them instantaneously. The release of a large number of molecules within a small volume of gas usually leads to a concentration increase by a factor of 1000 to 10,000, which opens the way to gas detection at the ppt-level at the cost of a longer response time. A few years ago, we developed a portable airborne-BTX sensor [1] by combining UV spectroscopy measurements and a pre-concentration stage; it has sensitivity in the low-ppb range that satisfies the requirements [2].

However, BTX compounds diluted in liquid samples also represent a threat and there are numerous potential sources, such as industrial spillage contaminating river basins and leaking underground storage tanks at aging gasoline stations contaminating the underground drinking water network. Despite the low solubility of BTX compounds in water, which limits their concentrations to low levels, the values given in Table 1 clearly show that such contamination remains a serious issue. Standard protocols for monitoring water quality have been developed using the same aforementioned techniques, so they exhibit the same limitations. To further extend the use of our portable airborne BTX sensor to liquid samples, we have developed modules that can be attached to the airborne system to provide an adequate interface with liquid samples. From theoretical considerations, UV spectroscopy can characterize liquid samples. However, because the molecules of interest interact with the solvent matrix, the absorption peaks are broader

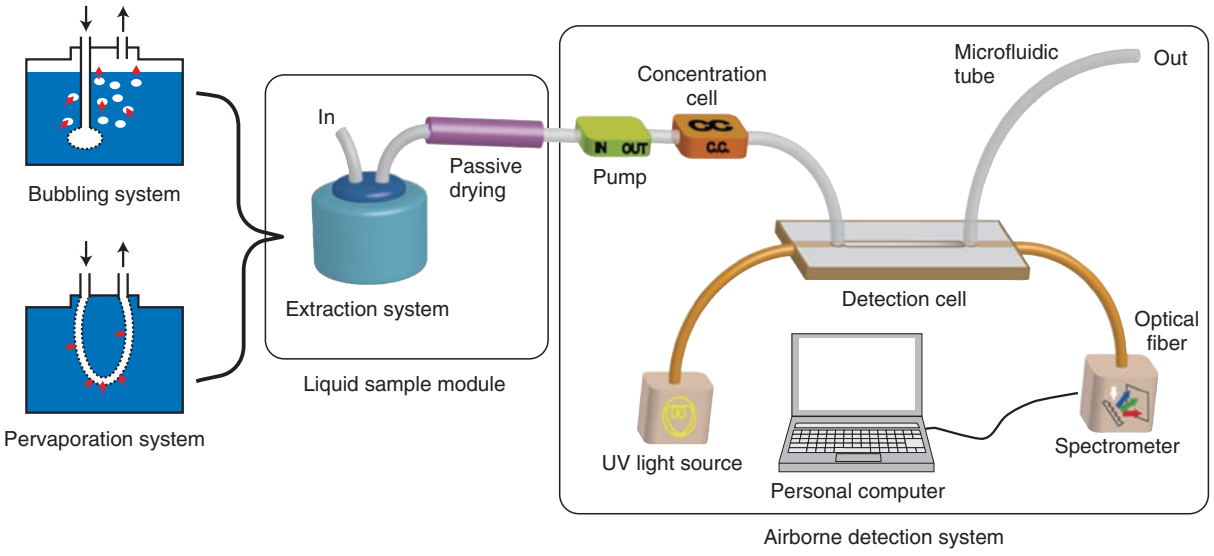

Fig. 2. Schematic view of the portable airborne BTX sensor combined with the liquid sample module, where the red arrows show the extraction path of BTX molecules.

and smaller, which makes sensitive and selective measurements much more challenging. This protocol thus operates much more efficiently with vapor-phase samples than liquid ones. To extend the use of our portable, high-sensitivity BTX sensor, we have developed two different extraction systems with specific properties (there is a tradeoff between sensitivity and selectivity) and a passive drying system that allows efficient use of the same pre-concentration stage as in the airborne system (**Fig. 2**).

2. Bubbling-based extraction module

As mentioned in the previous section, benzene, toluene, and o-xylene exhibit low affinity with water, so they are almost certain to evaporate as soon as their molecules are in close proximity to any air-liquid interface. The bubbling extraction technique takes advantage of this characteristic by increasing the air-liquid surface area to further enhance the evaporation of BTX molecules.

The concept has been extensively described elsewhere [3], but can be summarized as follows. Air as a carrier gas is pushed deep inside the sample liquid contained in a closed container. Air bubbles are then created deep inside the solution. As the bubbles rise to the surface, benzene molecules evaporate at the air bubble surface and accumulate within the bubble gas volume. When the bubbles reach the surface, they release their contents into the air in the overhead space, which is gradually transferred to the detection cell. With a large number of small bubbles, we can drastically increase the air-liquid surface ratio and extract the benzene from the entire volume of the sample liquid without any limitation from diffusion to the top surface. Experiments were performed with sample solutions prepared at known concentrations by diluting an adequate amount of pure solutions. Sample solutions were prepared in deionized water at concentration levels of 0.45, 3, and 3 ppmV (ppm by volume) for benzene, toluene, and o-xylene, respectively, where the benzene-to-toluene concentration ratio was fixed to match the levels expected from gasoline spillage. Experimental results obtained with the bubbling extraction module combined with the detection cell are shown in **Fig. 3**. The data show absorption peak heights at 253, 267, and 272 nm versus time for benzene, toluene, and o-xylene, respectively, with the time origin of 0 corresponding to when we started the carrier gas flow. The overall shapes of the curves in Fig. 3 are similar for the three BTX compounds, with maximum response reached after only a few minutes. This is consistent with an almost instantaneous extraction of BTX molecules, where the slow decrease in the response with elapsed time comes from the delay effect of the overhead volume. The extraction process is easy and fast, and its efficiency provides highly sensitive measurement of aqueous BTX.

However, this method has one issue concerning the

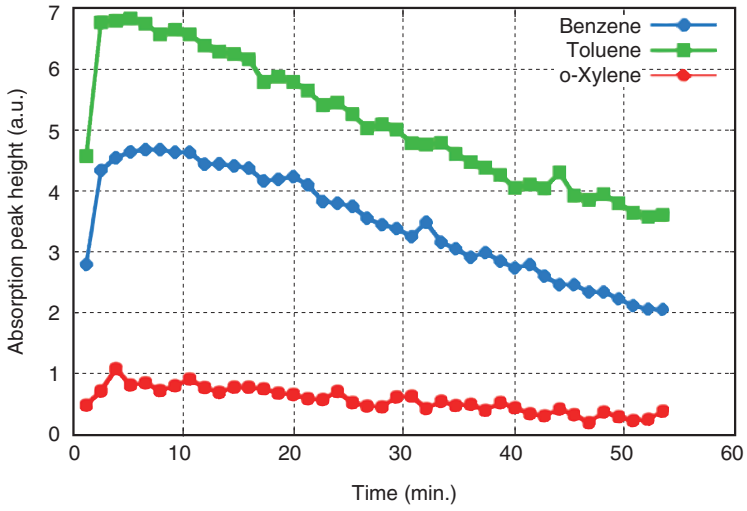

Fig. 3. Raw results for BTX sample solution with bubbling extraction and continuous monitoring by UV-spectroscopic measurements (no concentration stage).

selectivity to benzene. Many compounds exhibit low solubility in water and can thus be extracted efficiently to the gas phase by the bubbling protocol. Toluene is an ingredient of ordinary gasoline at a concentration level several times higher than that of benzene. Since toluene and o-xylene have absorption spectra that overlap that of benzene in the 230–290-nm range, their presence, as well as the presence of the potentially many other confounding molecules in real samples, may strongly interfere with benzene measurement, which requires better accuracy.

3. Pervaporation-based extraction module

An alternative extraction protocol based on a pervaporation technique [4] that provides better selectivity to benzene has been developed. Pervaporation occurs when a membrane separates the liquid phase feed and the vapor gas permeate and acts as a selective barrier. It combines two different basics processes: (1) from the liquid interface, permeation of the compound of interest through the membrane and (2) its evaporation into the vapor phase at the gas interface. Components are then separated on the basis of the difference in their transport rates through the membrane. Stronger affinity between the component and the membrane material yields faster extraction. As a result, hydrophobic membranes are commonly used to remove traces of organic compounds from aqueous solutions.

A typical pervaporation setup is shown in the left bottom of Fig. 2. A tube connects the gas inlet to the outlet and acts as a selective barrier between the liquid and gas phases. While flowing inside the tube, the carrier gas gathers the benzene molecules that have migrated through the tube wall and transports them towards the detection stage. Here, silicone rubber tubes, available on the market in various sizes at low cost, were used as pervaporation membranes. Experiments with calibrated BTX solutions were performed and typical results for BTX concentrations of 0.45 ppmV of benzene, 3 ppmV of toluene, and 3 ppmV of o-xylene are shown in **Fig. 4**. This time the extraction profiles strongly differed depending on the compound: benzene was extracted at a fast pace with a plateau reached after 30 min, toluene was gradually released from the silicone rubber at a slow and constant pace, and o-xylene was completely blocked by the membrane. As a consequence, within the first 15 min, the responses to benzene and toluene were about the same order of magnitude despite the huge disparities in their initial concentration levels. However, the plateau reached by the sensor response to benzene occurred at a level about three times lower than the maximum reported in Fig. 3, indicating a consequent loss of sensitivity.

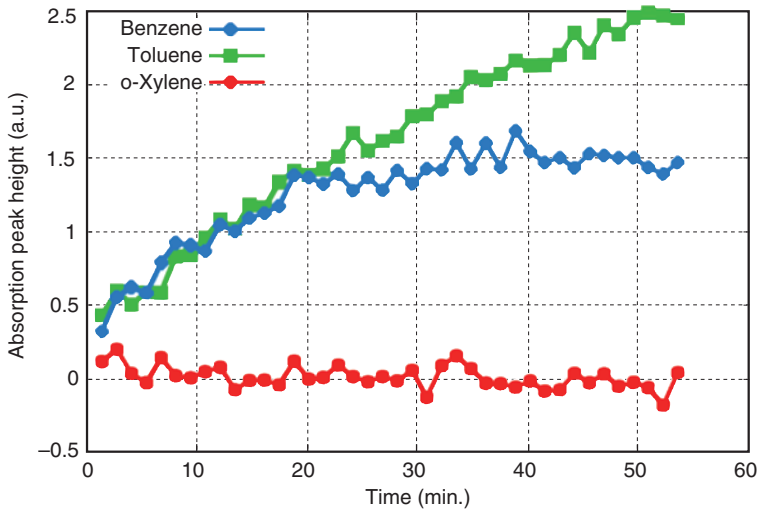

Fig. 4. Raw results for BTX sample solution with tube extraction and continuous monitoring by UV-spectroscopic measurements (no concentration stage).

4. Passive drying system for pre-concentration module

As a standard protocol in the gas-trace detection field, the pre-concentration technique has previously been implemented in our airborne-BTX portable sensor. However, after extraction from the liquid phase, the carrier gas coming out of the extraction module exhibited a relative humidity (RH) close to the saturation level, which strongly disturbed the efficiency of the pre-concentration cell through capillary condensation. To solve this problem, we added a passive drying system before the pre-concentration cell to selectively extract water molecules from the carrier gas. The passive drying system consists of a tube made of Nafion material [5]. When the carrier gas flows through this tube, the BTX molecules are retained inside the tube, while the water molecules as well as alcohols and a few other compounds can easily migrate through the Nafion membrane. This phenomenon, which is also called permeation, is equivalent to the pervaporation described earlier, but without the phase transition. As mentioned earlier, the extraction provides a carrier gas (air) with artificially high RH levels close to 100%, while the outer surface of the Nafion tube is exposed to ambient air at a RH of about 40–50%. To counterbalance the RH difference at the two sides of the Nafion membrane, the water molecules migrate through the membrane, from the inner space to the outer space. Because this phenomenon is fast and a small volume of carrier gas cannot change the RH value of the atmospheric gas surrounding the Nafion tube, this method enables one to get rid of excess water molecules, bringing the RH back to the atmospheric level, with a tube that is only a few centimeters long.

The typical gain in sensitivity when the pre-concentration stage is used in combination with bubbling extraction is shown in **Fig. 5**. Despite a short concentration time of 5 min, the overall response is shifted towards the low concentration levels by more than two orders of magnitude, leading to a detection limit in the pptV range, which far exceeds the requirements. The same effect has been reported with the tube-extraction system, but improvements are limited to low-ppbV levels. However, a better understanding of how the pre-concentration works would make possible further improvements in sensitivity. As mentioned above, the pre-concentration cell specifically accumulates the molecules of interest from the carrier gas over the so-called concentration time and then instantaneously releases them in a small volume of carrier gas for detection. The process can therefore be viewed as integration over the first few minutes of the chromatographic extraction response, as shown in Figs. 3 and 4 for bubbling and pervaporation extractions, respectively. In both cases, increasing the concentration time will improve the sensitivity at the cost of sensor response time but also impact the response selectivity to benzene. Therefore, from Figs. 3 and 4,

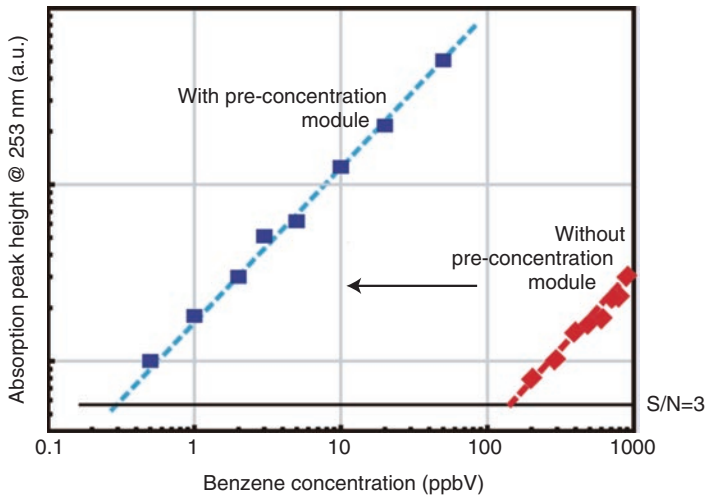

Fig. 5. Effect of the pre-concentration stage on sensor response with benzene aqueous solution and bubbling extraction (concentration time: 5 min).

we can expect two different behaviors: (1) with bubbling extraction, increasing the concentration time will slightly improve the sensitivity, and the selectivity to benzene will remain unchanged and (2) with pervaporation extraction, increasing the concentration time will drastically improve the sensitivity, but the selectivity to benzene will slightly decrease over the first 20 min and then decrease more rapidly for longer concentration times. Therefore, concentration time and choice of the extraction module are two factors that can be selected according to the application requirements in terms of sensor response, sensitivity, and selectivity to benzene.

5. Concluding remarks

We have developed a portable, high-sensitivity aqueous BTX sensor by adding two modules to the airborne-detection system: a system for extraction from the liquid phase to the vapor phase, followed by a passive drying system. Two extraction systems for different applications have been implemented and successfully tested. When high sensitivity is a priority, bubbling extraction should be chosen: the sensor response is relatively fast, and sensitivity in the pptV range can be tuned by means of the concentration time. However, when selectivity to benzene is the key feature, and other compounds such as toluene and o-xylene are also present at several times higher concentration levels, then the tube extraction system should be preferred. In future, field tests should be conducted to further validate the approach and demonstrate the ability of our sensor to perform realtime, on-site measurement at levels satisfying national regulations.

References

[1] T. Horiuchi, Y. Ueno, S. Camou, T. Haga, and A. Tate, "Portable Aromatic VOC Gas sensor for Onsite Continuous Air Monitoring with 10-ppb Benzene Detection Capability," NTT Technical Review, Vol. 4, No. 1, pp. 30-37, 2006. https://www.ntt-review.jp/archive/ntttechnical.php?contents=ntr200601030.pdf

[2] S. Camou, T. Horiuchi, and T. Haga, "Ppb Level Benzene Gas Detection by Portable BTX Sensor Based on Integrated Hollow Fiber Detection Cell," Proc. of IEEE Sensors 2006, Daegu, Korea, 2006.

[3] S. Camou, A. Shimizu, T. Horiuchi, and T. Haga, "Ppb-Level Detection of Benzene Diluted in Water with Portable Device Based on Bubbling Extraction and UV Spectroscopy," Sens. and Act. B, Vol. 32, No. 2, pp. 601–607, 2008.

[4] J. Amador-Hernandez and M. D. Luque de Castro, "Pervaporation: a Useful Tool in Food Analysis," Food Chemistry, Vol. 68, No. 4, pp. 387–394, 2000.

[5] P. W. Majsztrik, M. B. Satterfield, A. B. Bocarsly, and J. B. Benziger, "Water Sorption, Desorption and Transport in Nafion Membranes," J. of Membrane Science, Vol. 301, No. 1-2, pp. 93–106, 2007.

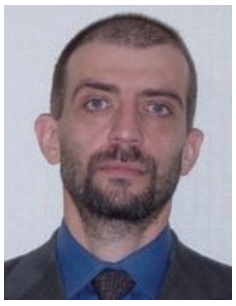

Serge Camou
Research Scientist, Network Hardware Integration Laboratory, NTT Microsystem Integration Laboratories.

He received the B.S., M.S., and Ph.D. degrees in physics from Cergy-Pontoise University, Paris 7 University, and Franche-Comte University, France, in 1994, 1996, and 2000, respectively. After two years as a JSPS (Japan Society for the Promotion of Science) fellow at the University of Tokyo doing research on DNA lab-on-a-chip devices, he moved to NTT Microsystem Integration Laboratories (Biosensing Group) in 2003 as a postdoctoral researcher and was involved in the airborne-BTX portable sensor development. In 2005, he was hired as a permanent researcher and is currently involved in the development of a noninvasive and continuous blood glucose system based on continuous-wave photoacoustic technology. He is a member of the IEEE Society.

Emi Tamechika
Senior Research Engineer, Supervisor, Leader of Microsensor Research Group, NTT Microsystem Integration Laboratories.

She received the B.S. and M.S. degrees in physics from Tokyo University of Science in 1983 and 1985, respectively, and the Ph.D. degree from Tokyo Metropolitan University in 1989. She joined NTT LSI Laboratories, Kanagawa, in 1989. She has been engaged in R&D of super-high-resolution improvement of optical lithography for LSI fabrication. She has also engaged in studies on silicon photonics technology. She received the Award of the Japanese Agency of Science and Technology for prominent patents in 1995. She is a member of the Japan Society of Applied Physics (JSAP), the Physical Society of Japan, the Electrochemical Society of Japan, and the Science Council of Japan.

Tsutomu Horiuchi
Senior Research Scientist, Network Hardware Integration Laboratory, NTT Microsystem Integration Laboratories.

He received the B.S. and M.S. degrees in physics from Waseda University, Tokyo, in 1983 and 1985, respectively. He received the Ph.D. degree in chemistry from Keio University, Kanagawa, in 1994. He joined NTT Ibaraki Electrical Communication Laboratories in 1985. He has been engaged in research on electrochemistry, biosensors, and chemical sensors. He was a visiting scientist at New Mexico State University, Las Cruces, NM, USA, in 1997. He is a member of JSAP.

Acoustically Controlled Spin Precession Revealed by Two-dimensional Imaging of Spin Transport in GaAs

Haruki Sanada†, *Hideki Gotoh, Koji Onomitsu, and Tetsuomi Sogawa*

Abstract

Magneto-optic Kerr microscopy was used to investigate the spin precession of electrons traveling in semiconductor quantum wells by using surface acoustic waves (SAWs). Two-dimensional images of the SAW-induced spin flow reveal anisotropic spin precession behavior caused by the coexistence of different types of spin-orbit interactions. The dependence of spin-orbit effective magnetic fields on SAW intensity indicates the existence of acoustically controllable spin-orbit interactions resulting from SAW-induced strain and SAW-induced Rashba contributions. These phenomena will provide the versatility needed for spin manipulation in future spintronic applications such as spin transistors and quantum computers.

1. Introduction

In conventional semiconductor electronics, electron spins have been ignored because they are randomly oriented and cancel out completely. The research field called *semiconductor spintronics* aims to extract spin properties in order to use them for both classical and quantum information technologies, which will achieve higher processing speeds, lower electrical power consumption, and higher integration densities than conventional charge-based devices [1]. Understanding the spin dynamics of electrons moving in semiconductors is one of the keys to developing spintronic technologies because it will enable electrical spin manipulation without external magnetic fields in ways that have been proposed for spin field-effect transistors [2], spin filters [3], and quantum computers [4]. In a system lacking inversion symmetry, moving electrons feel effective magnetic fields even in the absence of real magnetic fields. This is caused by spin-orbit interactions (SOIs) arising from relativistic effects. In general, magnetic fields induce spin precession, which is the rotation of the spin angular momentum around the magnetic field. Because of this, moving spins precess with a frequency proportional to the strength of the SOIs. So far, spin transport experiments using a DC-electric field [5] have succeeded in observing the spin precessions induced by SOIs in the absence of a real magnetic field [6]. Surface acoustic waves (SAWs) applied to semiconductor quantum wells (QWs), which confine electrons in thin layers sandwiched between barrier layers made of other materials, provide another way to transport electron spins [7]–[9]. This method has the advantage of effectively suppressing the dominant spin relaxation process caused by the electron-hole exchange interaction in undoped semiconductors [10] owing to the spatial separation of electrons and holes in the type-II-like lateral potential modulation created by the SAWs [7]. As a result, it has become possible to transport electrons by using SAWs over distances of nearly 100 μm while maintaining their spin coherence during precession around the effective magnetic fields caused by SOIs [8].

Here, we used magneto-optic Kerr rotation (KR)

† NTT Basic Research Laboratories
Atsugi-shi, 243-0198 Japan

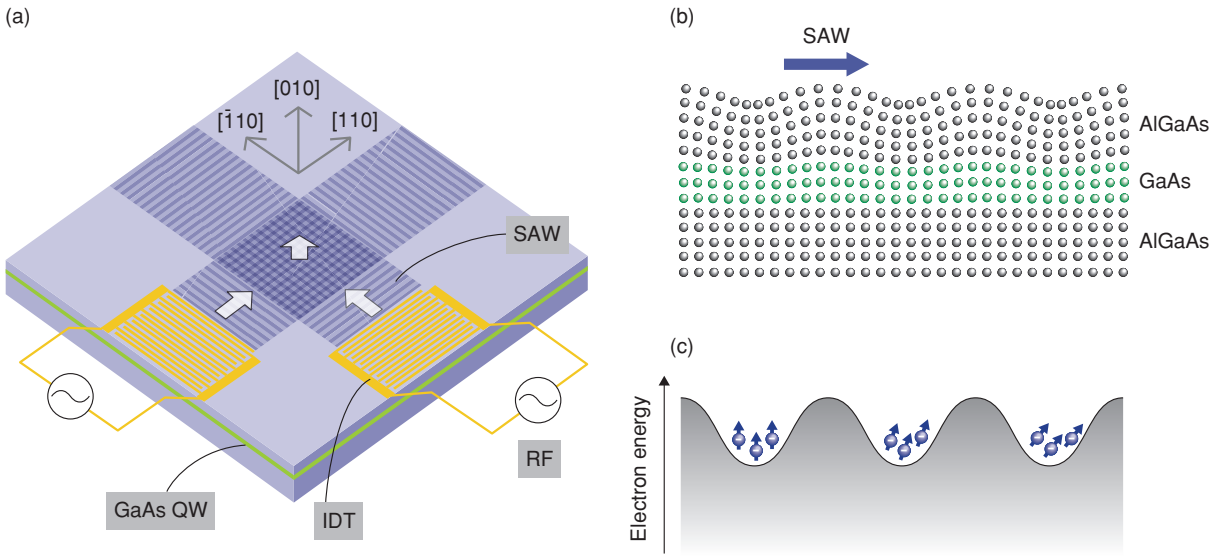

Fig. 1. (a) Schematic view of the sample. (b) SAW-induced displacement of atoms in the sample's cross section. Electrons are confined in a GaAs/AlGaAs QW. (c) Conduction band energy for the QW shown in (b). Electrons are trapped in the valleys of the modulated potential and transported by the SAWs.

microscopy to explore the two-dimensional (2D) dynamics of traveling spins under SAWs over a wide range of acoustic amplitudes. The present experiment revealed the existence of spatially anisotropic SOIs as well as their dependence on SAW strength. A theoretical analysis of the experimental results elucidated the mechanisms of the acoustically controllable spin dynamics. The phenomena will provide a new approach for the spin-manipulation as well as spin transport without the application of any magnetic fields or DC electric fields.

2. Experiment

A schematic view of the sample is shown in **Fig. 1(a)**. It was a 20-nm-thick undoped GaAs single QW with short-period GaAs/AlAs (average Al content: 30%) barriers grown by molecular-beam epitaxy on a (001) semi-insulating GaAs substrate. The QW was located 485 nm below the surface. A 50-nm-thick Al film deposited on top of the sample was processed by electron-beam lithography into interdigital transducers (IDTs), which were designed for operation at a SAW wavelength of 2.55 μm and frequency of 1.154 GHz. Rayleigh SAWs propagate along either [110] or [$\bar{1}$10], depending on the direction of the applied radio frequency (RF) signal, with a SAW velocity $|\mathbf{v}_{SAW}|$ = 2.9 km/s. The single SAW beams produce *moving wires*, which are formed by the one-dimensional (1D) lateral confinement of the SAW-induced piezoelectric potential (**Figs. 1(b)** and **(c)**). Interference between two orthogonal SAW beams forms *moving dots* traveling along [010] with a velocity of $\sqrt{2}\,|\mathbf{v}_{SAW}|$ [8], as shown in Fig. 1(a).

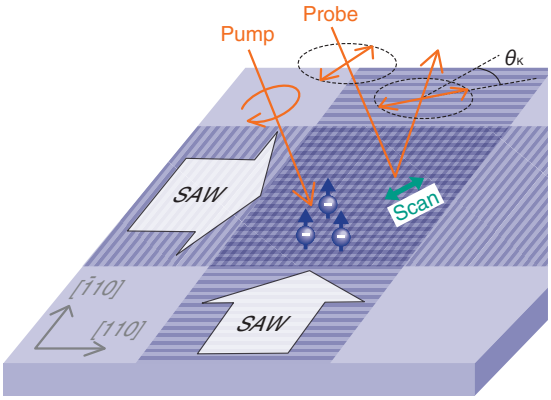

Fig. 2. Setup for spatially resolved KR measurements.

The spin dynamics during transport was measured by temporally and spatially resolved KR microscopy using a mode-locked Ti:sapphire laser (1.5 ps, 82 MHz, 1.527 eV), as illustrated in **Fig. 2**. Circularly polarized pump pulses (average power: 1.1 μW) were focused at a fixed position on the sample. Linearly polarized probe pulses (0.9 μW) with a time delay

relative to the pump pulses were scanned over the surface and the KR angle θ_K of their reflected light was measured by a balanced detection technique. The pump light's polarization was modulated between left- and right-circular polarizations at 50.1 kHz, and the probe light was chopped with an acousto-optic modulator at 52.0 kHz. The difference frequency (1.9 kHz) was used as a reference for lock-in detection. The full width at half maximum (FWHM) spot size of the normally incident probe beam was approximately 3 μm, whereas the waist size of the obliquely incident pump beam was 6 μm and its spot on the sample was slightly elongated in the [100] direction. The position of the probe light spot was scanned in the QW plane for spatially resolved KR measurements. For the 2D mapping of steady-state spin distributions, we chose to use a two-color pump-probe method using a pair of continuous-wave Ti: sapphire lasers. All the measurements were carried out at a low temperature (30 K), where long-distance spin transport is expected [7], [8] in the absence of applied magnetic fields.

3. Results and discussion

The spatiotemporal evolution of photoinjected spins trapped in moving dots traveling in the [010] direction is shown in **Fig. 3**. The slope of the KR signal indicates that the spin-polarized electrons moved with the expected velocity of $\sqrt{2}\,|\mathbf{v}_{SAW}| = 4.14$ km/s. The oscillations with a period of about 4.5 ns are attributed to spin precession around the spin-orbit effective magnetic field, as shown in the inset. The data thus clearly demonstrate that our method successfully extracted information about the spin dynamics, including spin transport and SOI-induced spin precession.

Spatial maps of steady-state spin densities for moving wires are shown in **Figs. 4(a)** and **(c)** and that for moving dots is shown in **Fig. 4(b)**. In the two-color measurement, the pump energy was fixed at 1.527 eV, whereas the probe energy was tuned to 1.525, 1.526, and 1.528 eV for [$\bar{1}$10], [010], and [110], respectively, because the bandgap energies at the electron-trapping positions were modulated by SAW fields [11]. The pump (probe) power was 20 (0.9) μW. In contrast to the well-confined carrier transport achieved by moving dots (Fig. 4(b)), carriers in moving wires diffused rapidly along the wire axis (Figs. 4(a) and (c)). Although the KR signal for the wires was reduced by the carrier diffusion, we could access the momentum direction dependences of spin precessions (**Fig. 4(d)**),

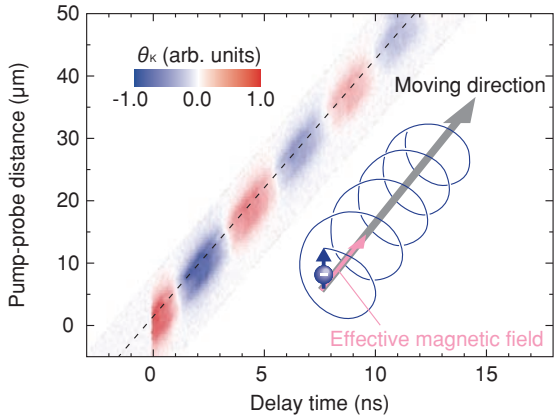

Fig. 3. Spatiotemporal evolution of the KR signal for moving dots traveling along [010]. The dashed line shows the slope determined from the estimated velocity of the moving dots. The inset shows the motion of the spin precessing around the effective magnetic field during transport.

where the sum of the mapping data (Figs. 4(a)–(c)) shows that the isophase lines have clear elliptical shapes. In **Fig. 4(e)**, the KR angles θ_K (open circles) along particular axes ([110], [010], and [$\bar{1}$10]) are fitted with a function $\theta_K(d)=\theta_0 \cos(2\pi\kappa d)\exp(-d/L_s)$, where d is the pump-probe distance and L_s and κ are fitting parameters representing the spin decay length and spatial precession frequency, respectively. We obtained $\kappa_{[110]} = 0.0589 \pm 0.0008$, $\kappa_{[010]} = 0.05369 \pm 0.00009$, and $\kappa_{[\bar{1}10]} = 0.0460 \pm 0.0006$ μm^{-1} for the traveling directions [110], [010], and [$\bar{1}$10], respectively. Since κ is proportional to the spin-orbit effective magnetic field, these results demonstrate that the SOIs are spatially anisotropic in the present system.

The SOI dependence on the traveling direction is caused by the coexistence of different types of SOIs [6], [12]–[14]. For electrons confined in (001) QWs, the momentum-dependent effective magnetic field $\Omega_{so}(\mathbf{k})$is primarily determined by k-linear terms, which are classified into two types [15]:

$$\Omega^{\alpha}(\mathbf{k})=\frac{2\alpha}{\hbar}\begin{bmatrix} k_Y \\ -k_X \\ 0 \end{bmatrix},\quad \Omega^{\beta}(\mathbf{k})=\frac{2\beta}{\hbar}\begin{bmatrix} -k_X \\ k_Y \\ 0 \end{bmatrix}, \qquad (1)$$

where we used a coordinate system with base vectors $\hat{\mathbf{X}}$ // [100], $\hat{\mathbf{Y}}$ // [010], and $\hat{\mathbf{Z}}$ // [001]. The orientation dependences of $\Omega^{\alpha}(\mathbf{k})$ and $\Omega^{\beta}(\mathbf{k})$ in $\mathbf{k}$ space are shown in **Fig. 5**. Since these vectors have different dependences on the direction of $\mathbf{k}$, their coexistence

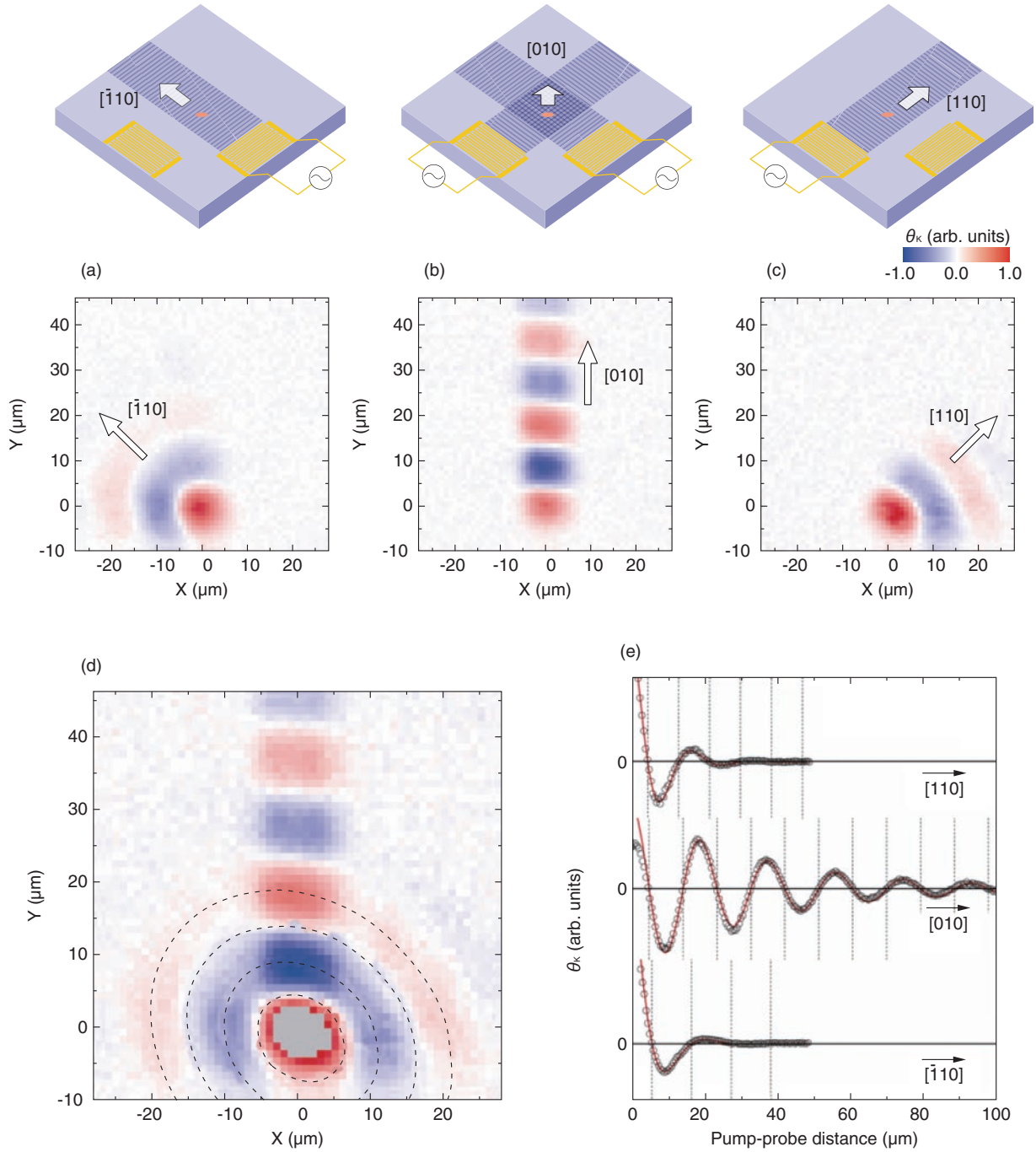

Fig. 4. (a)–(d) 2D images of spin densities for moving wires traveling along [$\bar{1}$10] (a) and [110] (c) and for moving dots traveling along [010] (b). The sum of the data (a)–(c) is plotted in (d), where the dashed ellipses are guides for the eye. (e) Kerr rotation signals along the three directions in the data (a)–(c) are plotted (black open circles) and the red lines are fitting curves. The dashed lines represent precession phases of π/2, (3/2)π, (5/2)π, ...

leads to twofold symmetry of $|\Omega^{total}(\mathbf{k})|=|\Omega^{\alpha}(\mathbf{k})+\Omega^{\beta}(\mathbf{k})|$, as illustrated in Fig. 5. In general, $\Omega^{\alpha}(\mathbf{k})$ and $\Omega^{\beta}(\mathbf{k})$ are mainly induced by the structural inversion asymmetry caused by a static electric field (Rashba SOI [16]) and the intrinsic bulk inversion asymmetry (Dresselhaus SOI [17]), respectively. In addition to

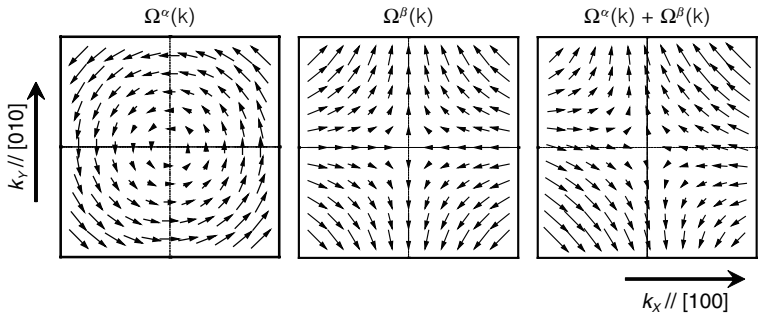

Fig. 5. Effective magnetic fields $\mathbf{\Omega}^{\alpha}$, $\mathbf{\Omega}^{\beta}$, and $\mathbf{\Omega}^{\alpha} + \mathbf{\Omega}^{\beta}$ plotted as vectors in **k** space. $\alpha < 0$, $\beta > 0$, and $\beta > |\alpha|$ are assumed in this figure.

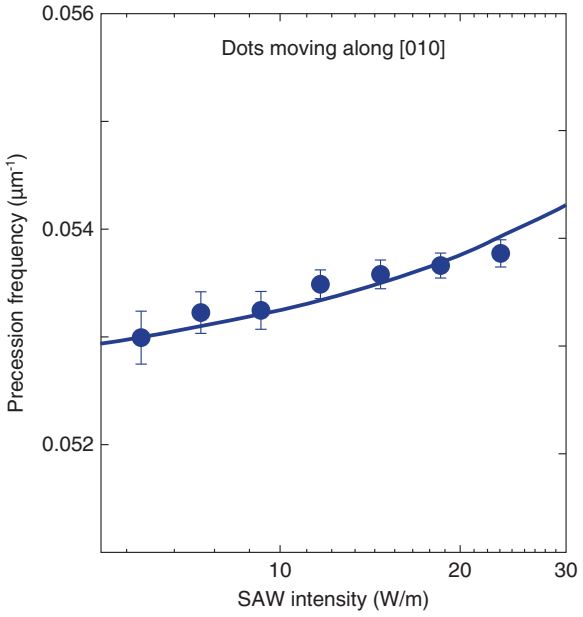

Fig. 6. SAW intensity dependence of precession frequency for moving dots. The solid line was obtained by calculation. The error bars for the data represent two standard errors of the parameters obtained from a least-squares fitting.

these static contributions, the present system should have a dynamic Rashba SOI induced by the vertical component of the SAW piezoelectric field as well as strain-induced SOIs [18]–[20].

As expected, the precession frequency varied with the SAW intensity, which is defined as the acoustic power flux per unit length along a cross-section of the SAW beam. The symbols in **Fig. 6** represent the experimentally obtained precession frequency as a function of the SAW intensity for moving dots. We estimated the SAW intensities from the bandgap shift observed in photoluminescence spectra [21]. As the SAW intensity increased, the precession frequency increased monotonically, suggesting that the SOI is acoustically controllable. The experimental data were well reproduced by simulating the precession frequency (solid lines in Fig. 6) [22], where each SOI contribution to the spin precessions was estimated from the calculation of the Rayleigh SAW fields including the piezoelectric coupling [23]. This analysis revealed the contributions of SAW-dependent Rashba and strain SOIs to the total SOI, indicating that the spin rotation angle can be tuned by adjusting the SAW intensity.

4. Conclusion

We studied the SOIs of electrons traveling in semiconductor QWs by using SAW fields. The temporally and/or spatially resolved KR technique enabled 2D imaging of the traveling spins, which revealed anisotropic spin precession behavior resulting from the coexistence of different types of SOIs. The dependence of the precession frequencies on SAW intensity, which was analyzed on the basis of a theoretical model, indicates that the strengths of the SOIs due to strain and Rashba contributions can be tuned by adjusting the SAW intensity. Our experimental results will be beneficial for further investigation of acoustically induced SOIs in semiconductors. They will also provide the versatility needed for spin manipulation via dynamically controlled SOIs in future spintronic applications such as spin transistors and quantum computers.

Acknowledgments

We thank P. V. Santos of Paul-Drude-Institut für Festkörperelektronik, Berlin, Germany, and J. Nitta and M. Kohda of Department of Materials Science, Tohoku University, Sendai, Japan, for useful discussions. This work was partly supported by the Japan Society for the Promotion of Science (JSPS).

References

[1] S. A. Wolf, D. D. Awschalom, R. A. Buhrman, J. M. Daughton, S. von Molnár, M. L. Roukes, A. Y. Chtchelkanova, and D. M. Treger, "Spintronics: A Spin-based Electronics Vision for the Future," Science, Vol. 294, pp. 1488–1495, 2001.

[2] S. Datta and B. Das, "Electronic Analog of the Electro-optic Modulator," Appl. Phys. Lett., Vol. 56, No. 7, p. 665, 1990.

[3] T. Koga and S. Datta, "Spin-filter Device Based on the Rashba Effect Using a Nonmagnetic Resonant Tunneling Diode," Phys. Rev. Lett., Vol. 88, No. 12, p. 126601, 2002; J. Ohe, M. Yamamoto, T. Ohtsuki, and J. Nitta, "Mesoscopic Stern-Gerlach Spin Filter by Nonuniform Spin-orbit Interaction," Phys. Rev. B, Vol. 72, No. 12, p. 041308, 2005.

[4] D. Stepanenko and N. E. Bonesteel, "Universal Quantum Computation through Control of Spin-orbit Coupling," Phys. Rev. Lett., Vol. 93, No. 14, p. 140501, 2004.

[5] J. M. Kikkawa and D. D. Awschalom, "Lateral Drag of Spin Coherence in Gallium Arsenide," Nature (London) Vol. 397, No. 6715, p. 139, 1999; D. Hägele, M. Oestreich, W. W. Rühle, N. Nestle, and K. Eberl, "Spin Transport in GaAs," Appl. Phys. Lett., Vol. 73, No. 11, p. 1580, 1998; H. Sanada, I. Arata, Y. Ohno, Z. Chen, K. Kayanuma, Y. Oka, F. Matsukura, and H. Ohno, "Relaxation of Photoinjected Spins during Drift Transport in GaAs," Appl. Phys. Lett., Vol. 81, No. 15, p. 2788, 2002.

[6] Y. Kato, R. C. Myers, A. C. Gossard, and D. D. Awschalom, "Coherent Spin Manipulation without Magnetic Fields in Strained Semiconductors," Nature (London), Vol. 427, No. 6969, p. 50, 2004.

[7] T. Sogawa, P. V. Santos, S. K. Zhang, S. Eshlaghi, A. D. Wieck, and K. H. Ploog, "Transport and Lifetime Enhancement of Photoexcited Spins in GaAs by Surface Acoustic Waves," Phys. Rev. Lett., Vol. 87, No. 27, p. 276601, 2001.

[8] J. A. H. Stotz, R. Hey, P. V. Santos, and K. H. Ploog, "Coherent Spin Transport through Dynamic Quantum Dots," Nature Mater., Vol. 4, No. 8, p. 585, 2005.

[9] O. D. D. Couto, Jr., F. Iikawa, J. Rudolph, R. Hey, and P. V. Santos, "Anisotropic Spin Transport in (110) GaAs Quantum Wells," Phys. Rev. Lett., Vol. 98, No. 3, p. 036603, 2007.

[10] G. L. Bir, A. G. Aronov, and G. E. Pikus, "Spin Relaxation of Electrons due to Scattering by Holes," Zh. Eksp. Teor. Fiz. Vol. 69, No. 4, p. 1382, 1975 [Sov. Phys. JETP, Vol. 42, p. 705, 1975].

[11] F. Alsina, P.V. Santos, and R. Hey, "Spatial-dispersion-induced Acoustic Anisotropy in Semiconductor Structures," Phys. Rev. B, Vol. 65, No. 19, p. 193301, 2002.

[12] L. Meier, G. Salis, I. Shorubalko, E. Gini, S. Schön, and K. Ensslin, "Measurement of Rashba and Dresselhaus Spin-orbit Magnetic Fields," Nature Phys., Vol. 3, No. 9, p. 650, 2007.

[13] B. M. Norman, C. J. Trowbridge, J. Stephens, A. C. Gossard, D. D. Awschalom, and V. Sih, "Mapping Spin-orbit Splitting in Strained (In,Ga)As Epilayers," Phys. Rev. B, Vol. 82, No. 8, p. 081304(R), 2010.

[14] S. D. Ganichev, V. V. Bel'kov, L. E. Golub, E. L. Ivchenko, P. Schneider, S. Giglberger, J. Eroms, J. De Boeck, G. Borghs, W. Wegscheider, D. Weiss, and W. Prettl, "Experimental Separation of Rashba and Dresselhaus Spin Splittings in Semiconductor Quantum Wells," Phys. Rev. Lett., Vol. 92, No. 25, p. 256601, 2004; M. Scheid, M. Kohda, Y. Kunihashi, K. Richter, and J. Nitta, "All-electrical Detection of the Relative Strength of Rashba and Dresselhaus Spin-orbit Interaction in Quantum Wires," Phys. Rev. Lett., Vol. 101, No. 26, p. 266401, 2008; M. Studer, G. Salis, K. Ensslin, D. C. Driscoll, and A. C. Gossard, "Gate-controlled Spin-orbit Interaction in a Parabolic GaAs/AlGaAs Quantum Well," Phys. Rev. Lett., Vol. 103, No. 2, p. 027201, 2009.

[15] R. Winkler, "Spin-orbit Coupling Effects in Two-dimensional Electron and Hole Systems," Springer, Berlin, 2003.

[16] Y. A. Bychkov and E. I. Rashba, "Oscillatory Effects and the Magnetic Susceptibility of Carriers in Inversion Layers," J. of Physics C: Solid State Physics, Vol. 17, No. 33, p. 6039, 1984.

[17] G. Dresselhaus, "Spin-orbit Coupling Effects in Zinc Blende Structures," Phys. Rev. Vol. 100, No. 2, pp. 580–586, 1955.

[18] G. E. Pikus and A. N. Titkov, in "Optical Orientation," edited by F. Meier and B. P. Zakharchenya, Elsevier, Amsterdam, 1984.

[19] G. C. La Rocca, N. Kim, and S. Rodriguez, "Effect of Uniaxial Stress on the Electron Spin Resonance in Zinc-blende Semiconductors," Phys. Rev. B, Vol. 38, No. 11, pp. 7595–7601, 1988.

[20] B. A. Bernevig and S.-C. Zhang, "Spin Splitting and Spin Current in Strained Bulk Semiconductors," Phys. Rev. B, Vol. 72, No. 11. p. 115204, 2005.

[21] T. Sogawa, P. V. Santos, S. K. Zhang, S. Eshlaghi, A. D. Wieck, and K. H. Ploog, "Dynamic Band-structure Modulation of Quantum Wells by Surface Acoustic Waves," Phys. Rev. B, Vol. 63, No. 12, p. 121307(R), 2001.

[22] H. Sanada, T. Sogawa, H. Gotoh, K. Onomitsu, M. Kohda, J. Nitta, and P. V. Santos, "Acoustically Induced Spin-orbit Interactions Revealed by Two-dimensional Imaging of Spin Transport in GaAs," Phys. Rev. Lett., Vol. 106, No. 21, p. 216602, 2011.

[23] S. H. Simon, "Coupling of Surface Acoustic Waves to a Two-dimensional Electron Gas," Phys. Rev. B, Vol. 54, No. 19, p. 13878, 1996.

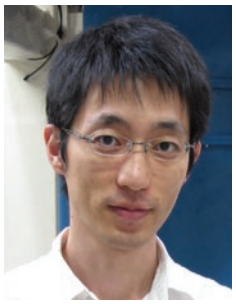

Haruki Sanada

Research Scientist, Quantum Optical Physics Research Group, Optical Science Laboratory, NTT Basic Research Laboratories.

He received the B.E., M.E., and Ph.D. degrees in electrical engineering from Tohoku University, Miyagi, in 2001, 2002, and 2005, respectively. He joined NTT Basic Research Laboratories in 2005. His research interests include the optical properties of low-dimensional semiconductor nanostructures and carrier spin dynamics modulated by surface acoustic waves and their application to solid-state quantum information processing. He is a member of the Japan Society of Applied Physics (JSAP).

Hideki Gotoh

Senior Research Scientist, NTT Basic Research Laboratories.

He received the B.E., M.E., and Ph.D. degrees in engineering from Hiroshima University in 1991, 1993, and 2000, respectively. Since joining NTT Basic Research Laboratories in 1993, he has been working on optical physics and device applications of semiconductor nanostructures. He is a member of JSAP and the Optical Society of America.

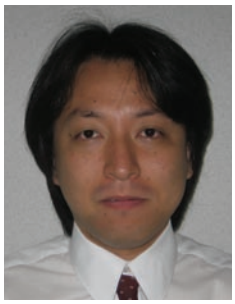

Koji Onomitsu

Research Scientist, Nanostructure Technology Research Group, Physical Science Laboratory, NTT Basic Research Laboratories.

He received the B.E. and M.E. degrees in electrical engineering from Aoyama Gakuin University, Tokyo, in 1998 and 2000, respectively, and the Ph.D. degree in electrical engineering from Waseda University, Tokyo, in 2004. He joined NTT Basic Research Laboratories in 2006. His current interests are crystal growth of modulation doped structures for high-mobility two-dimensional electron systems using MBE, mechanical devices incorporating GaMnAs, and on-chip amplifiers of mechanical vibration signals using HEMTs. He is a member of JSAP.

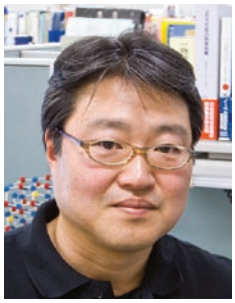

Tetsuomi Sogawa

Executive Manager of Research Planning Section, and Group Leader of Quantum Optical Physics Research Group, NTT Basic Research Laboratories.

He received the B.E., M.E., and Ph.D. degrees in electrical engineering from the University of Tokyo in 1986, 1988, and 1991, respectively. He joined NTT Basic Research Laboratories in 1991. From 2004 to 2006, he worked for the Council for Science and Technology Policy, Cabinet Office, Japan, as a deputy director for policy planning. His current research interests include fabrication technology for low-dimensional nanostructures, optical properties of quantum dots/wires and photonic crystals, spin-related phenomena, and SAW application to nanostructures. He is a member of JSAP.

Damage to Plastic Components Caused by Solvent Cracking

Abstract

This article introduces two case studies of damage to plastic components caused by solvent cracking and the countermeasures developed by NTT EAST. It is the ninth in a bimonthly series on the theme of practical field information about telecommunication technologies. This month's contribution is from the Materials Engineering Group, Technical Assistance and Support Center, Maintenance and Service Operations Department, Network Business Headquarters.

1. Introduction

Telecommunication facilities use various materials such as metal, concrete, and plastic. Among these, plastic is widely used in equipment that comes into direct contact with customers. This article introduces two case studies of how plastic components can be damaged and the countermeasures that were taken to prevent reoccurrence.

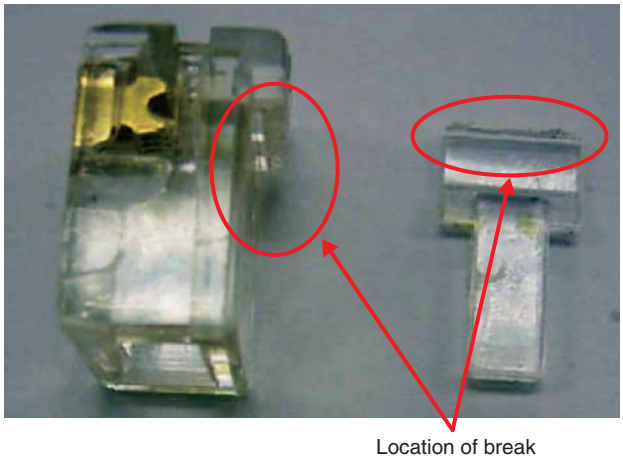

Fig. 1. Modular plug with damaged latching tab.

† NTT EAST
Ota-ku, 144-0053 Japan

2. Damage to latching tab of modular plug

2.1 Problem

At a certain metalworking plant in Japan, the modular plug of the helical cord of a particular telephone receiver had to be replaced repeatedly because the plug's latching tab broke away from its base three times over the course of a five-year period (**Fig. 1**). The telephone set sat on a desk on the work floor and traces of cutting oil used for cutting metal plates on a lathe could be seen splattered about the desk. Grease from this cutting oil was also found on the telephone's helical cord (**Fig. 2**). The damaged modular plug was

Fig. 2. Helical cord stained with grease from cutting oil.

made of acrylic resin.

2.2 Cause of damage

Some plastic materials are known to suffer from cracking when solvents or oils adhere to locations subjected to stress. This solvent cracking is a type of environmental-stress cracking that affects plastic molded products. If a large amount of internal stress (strain) exists in a molded product that comes into contact with solvents or oils, those substances may penetrate into the product and cause intermolecular slippage and crack generation. This is accompanied by molecular exfoliation that gives rise to a highly glossy, mirror-like fractured surface.

In this case study, the plug's acrylic resin had low resistance to solvent cracking and cutting oil was found on the plug, so two of the key conditions for crack generation were present.

The fractured surface of the damaged plug was observed with a digital microscope and found to be highly glossy and mirror-like without any unevenness (**Fig. 3**), which is a characteristic feature of solvent cracking.

To continue our investigation, we conducted an experiment to reproduce such solvent cracking using the same type of cutting oil as used at the metalworking plant. When the receiver of a telephone set is lifted off its hook, the cord is stretched, which applies stress to the latching tab, which pushes it away from its base. To simulate this process, we coated the latching tab of a new modular plug with cutting oil, applied stress to the tab's base, and heated the tab at 80°C using a Geer oven to accelerate the reaction. After two weeks, cracks occurred at the base. Digital microscope observation of the fractured surface revealed a smooth, mirror-like surface similar to the fractured surface of the actual damaged tab at the metalworking plant (**Fig. 4**).

2.3 Measures to prevent reoccurrence

Connecting a modular plug to the modular socket on a receiver that has been splashed with cutting oil may cause the plug's tab to eventually break away owing to ongoing damage caused by remnant oil. Therefore, the socket should be wiped clean of remnant grease with a cotton swab or other implement before the plug is inserted. We also recommend using a gel to fill the gap in the plug's aperture where the spiral cord is inserted to prevent cutting oil from entering the socket.

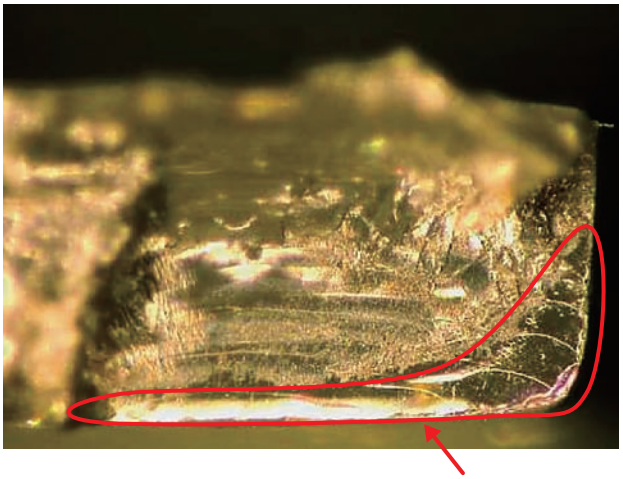

Fig. 3. Fractured surface of modular plug damaged at metalworking plant.

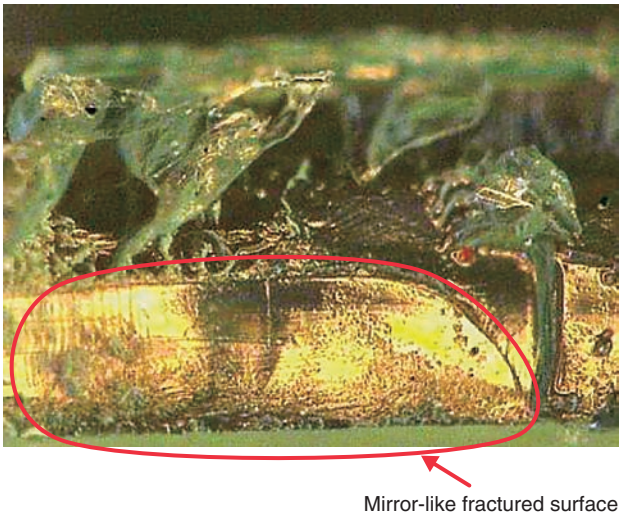

Fig. 4. Experimentally reproduced fractured surface.

3. Damage to connector of AC adaptor for ISDN modem

3.1 Problem

In response to a fault report stating that power could not be supplied to an ISDN (integrated services digital network) modem, an inspection found that the connector of the modem's AC adaptor was damaged (**Fig. 5**). Further inspection also found the remains of ants in the socket-pin area and on the nearby circuit board, as shown in **Fig. 6**. There had been no reports

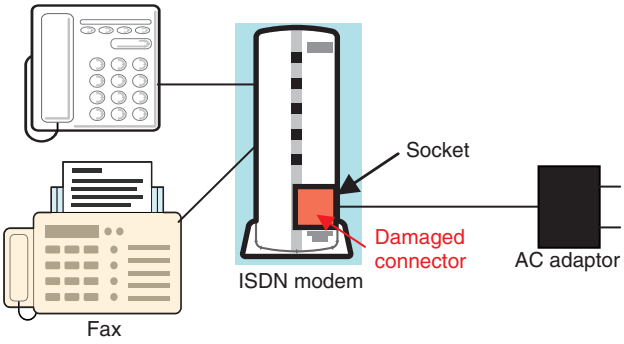

Fig. 5. Location of damaged connector.

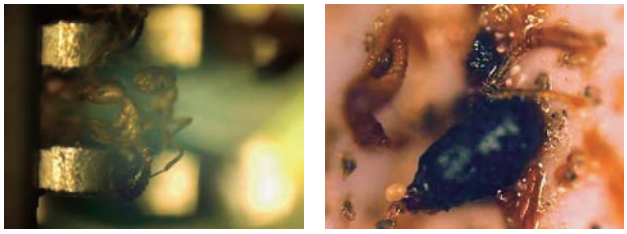

Fig. 6. Ant that penetrated ISDN modem.

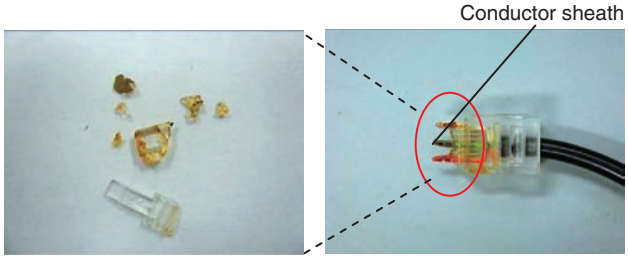

Fig. 7. Damaged AC-adaptor connector.

of lightning strikes or power outages since the installation of this equipment.

3.2 Inspection results

The connector (made of polycarbonate material) was found to have fallen to pieces, exposing the sheathing of its conducting wires (**Fig. 7**). Moreover, the sheathing (made of flexible polyvinyl chloride) was also found to have surface sores (**Fig. 8**). A brownish adherent thought to be the remains of ants

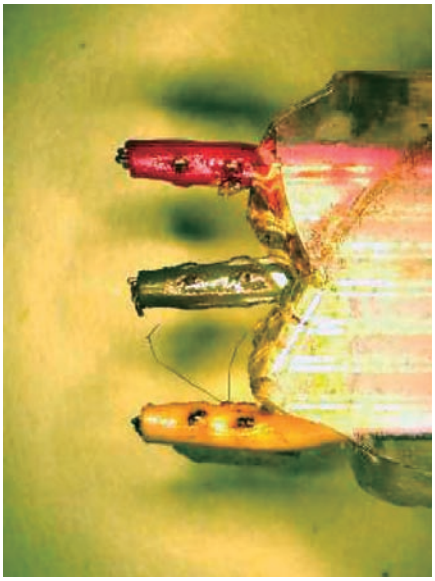

Fig. 8. Sores on conductor sheaths inside connector.

Table 1. Results of ion chromatography analysis of substance in damaged connector.

Unit: ppm

	F^-	$HCOO^-$	Cl^-	NO_2^-	NO_3^-	PO_4^{3-}	SO_4^{2-}
1st run	4.96	28.60	20.61	3.43	2.72	5.40	7.32
2nd run	5.15	30.45	21.55	3.80	3.21	5.21	7.75
Average	5.15	29.53	21.55	3.80	3.21	5.30	7.75

was found inside the damaged connector and the charred remains of an ant were found on the circuit board near the socket.

3.3 Cause of damage

We analyzed the brownish adherent in the damaged connector by ion chromatography and found the presence of formic acid ($HCOO^-$), as indicated in **Table 1**. While connector damage due to formic acid was therefore suspect, microscopic observation of the connector at the breaks revealed smooth, mirror-like fractured surfaces. We therefore investigated the possibility that solvent cracking was the cause of this damage. The abovementioned charred ant remains found on the circuit board near the socket led us to believe that an ant had entered through gaps in the modem's enclosure and made contact with metal pins causing an electrical short and consequently generating high temperatures. Furthermore, taking into

account the presence of sores on conductor sheaths near that circuit board, we considered that those sheaths were also heated when the electrical circuit shorted. We therefore surmised that the heating of conductor sheaths in this way could cause plasticizing agent to separate from the sheath and come into contact with the polycarbonate connector, thereby generating solvent cracking. Infrared reflection spectroscopic measurements of these conductor sheaths confirmed the presence of a phthalate ester plasticizer. The penetration of phthalate ester plasticizer into polycarbonate resin is known to facilitate solvent cracking. We therefore concluded that solvent cracking was probably the reason for the damage to the AC-adaptor connector in this case study.

4. Conclusion

This article introduced case studies of damage to plastic components caused by solvent cracking. When materials that contain solvents (such as adhesives, paints, and oils) are used near equipment containing plastic components, special care must be taken to ensure that such materials do not adhere to the equipment. We hope that this article has been useful in helping the reader obtain a better understanding of material deterioration.

NTT Receives Award from the Thomson Reuters 2011 Top 100 Global Innovators Program

Nippon Telegraph and Telephone Corporation (NTT, Tokyo) has received an award from the Thomson Reuters 2011 Top 100 Global Innovators program [1], [2]. This program launched by Thomson Reuters (New York) is an initiative that analyzes patent data and related metrics using a proprietary methodology to identify the companies and institutions that lead the world in innovation. The methodology is based on four principal criteria: patent approval success rate*1, global reach of patent portfolio*2, patent influence in literature citations*3, and overall patent volume. Thomson Reuters state that "being recognized as a Top 100 Global Innovator … confirms an organization's commitment to progressing innovation globally, to the protection of ideas and to the commercialization of inventions."

NTT understands that this award certifies that its R&D activities are pioneering and its inventions are valuable in the global market. It will make every effort to promote patent acquisition based on the outputs of R&D activities and make the most use of owning intellectual properties.

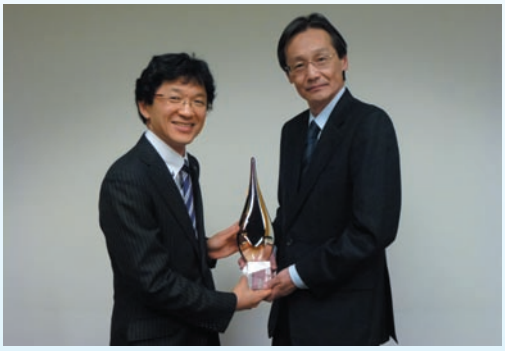

Haruhiko Kojima (left), Managing Director, NTT Intellectual Property Center, receiving a trophy from Masaki Nagao (right), Managing Director, Thomson Reuters Professional KK, a Thomson Reuters Company.

References

[1] NTT Technical Review.
https://www.ntt-review.jp/archive/ntttechnical.php?contents=ntr201201ext.html

[2] Thomson Reuters Names World's 100 Most Innovative Companies
http://thomsonreuters.com/content/press_room/legal/515197

*1 Patent approval success rate: the ratio of published applications to granted patents over the most recent three years.

*2 Global reach of patent portfolio: the metric calculated by using the number of innovative patents that have quadrilateral patents (China, Europe, Japan, and the USA). An innovative patent is defined as the first publication in a patent document of a new technology etc.

*3 Patent influence in literature citations: the metric determined by counting citations to each organization's patents over the most recent five years, excluding self-citations.

External Awards

SAINT2011 Best Paper Award

Winners: Mitsuaki Akiyama, Takeshi Yagi, and Mitsutaka Ito, NTT Information Sharing Platform Laboratories
Date: July 19, 2011
Organization: IEEE/IPSJ

For "Searching Structural Neighborhood of Malicious URLs to Improve Blacklisting".

Filtering based on blacklists is a major countermeasure against malicious websites. However, blacklists must be updated because malicious URLs (uniform resource locators) tend to be short-lived and their sub strings may be partially mutated to avoid blacklisting. Due to these characteristics, it can be assumed that unknown malicious URLs exist in the neighborhood of known malicious URLs, created by the same adversary. We propose an effective blacklist URL generation method. We try to discover URLs in the neighborhood of a malicious URL by using a search engine. Those suspicious neighborhoods around malicious URLs require further investigation to determine their blacklisting candidacy. We experimentally evaluated this generation method by using real blacklisted URLs for both drive-by-download and click-download infection. The results showed that our method can effectively improve identification of malicious URLs and maintenance of the coverage of blacklists.

Published as: M. Akiyama, T. Yagi, and M. Itoh, "Searching Structural Neighborhood of Malicious URLs to Improve Blacklisting," Proc. of the 2011 IEEE/IPSJ 11th International Symposium on Applications and the Internet (SAINT), pp. 1–10, Munich, Bavaria.

IEICE Distinguished Service Award

Winner: Takashi Ikebe, Service Control Platform Development Project, Third Promotion Project, NTT Network Service Systems Laboratories
Date: Sep. 14, 2011
Organization: IEICE Communications Society

For contributions to conducting conferences for the technical committee on network systems as an assistant to the Secretary General.